

UCSF

UC San Francisco Electronic Theses and Dissertations

Title

Genetic and Cellular Interactions That Shape The Zebrafish Retinotectal Projection

Permalink

<https://escholarship.org/uc/item/3d4749v5>

Author

Gosse, Nathan John

Publication Date

2008-01-09

Peer reviewed|Thesis/dissertation

Genetic and Cellular Interactions That Shape The Zebrafish Retinotectal Projection

by

Nathan J. Gosse

DISSERTATION

Submitted in partial satisfaction of the requirements for the degree of

DOCTOR OF PHILOSOPHY

in

Genetics / Developmental Biology

in the

GRADUATE DIVISION

of the

UNIVERSITY OF CALIFORNIA, SAN FRANCISCO

UMI Number: 3289323

Copyright 2008 by
Gosse, Nathan J.

All rights reserved.

UMI[®]

UMI Microform 3289323

Copyright 2008 by ProQuest Information and Learning Company.
All rights reserved. This microform edition is protected against
unauthorized copying under Title 17, United States Code.

ProQuest Information and Learning Company
300 North Zeeb Road
P.O. Box 1346
Ann Arbor, MI 48106-1346

Copyright 2008

by

Nathan J. Gosse

PREFACE

This work would not have been possible without the support, guidance, generosity, and patience exhibited by a great number of people over the past few years. At the cost of omitting many others deserving of additional thanks, I would like to acknowledge the contributions of the following people:

My parents, Jon and Jodi, who have motivated me to push myself and discover, with support and enthusiasm, from the start.

My brothers, Dave and Joe, who have been my trustiest collaborators in all endeavors scientific or otherwise.

My labmates, teammates, and classmates at UCSF, who could be more accurately described as my friends, for consistently offering support, constructive criticism, and an avenue for release.

My mentor, Herwig, for his demonstrations of how to think in an open-minded but focused manner, how to build results into a story, and how to thrive on (and even enjoy) the challenges of benchwork.

My wife, Julie, who has given me a gleaming example of success, a smiling reason to aspire toward it, the caring support to do so, and when necessary, a loving nudge to make sure it happens. Nothing could be better than knowing we have a lifetime to spend together.

ABSTRACT

Genetic and Cellular Interactions That Shape The Zebrafish Retinotectal Projection

The retinotectal projection has long served as an experimentally accessible model for the study of topographic map formation and function. Retinal ganglion cells (RGCs) project to their midbrain target, the optic tectum, such that neighbor relationships are preserved between pre- and postsynaptic cells.

Organization of the map relies on first establishing positional information in the retina and tectum. Differentiating cells in the developing eye must be coded with positional information, giving them a molecular identity along the dorsal-ventral (DV), and anterior posterior (AP) axis. The DV relies on a cascade of secreted signalling factors which establish domains of expression for dorsal-specific and ventral-specific transcription factors. Through a behavioral forward genetic screen, we have identified a mutant, *s327*, with an aberrant retinotectal projection. The unusual projection arises as a result of defective retinal patterning, specifically lacking expression of the dorsal marker *tbx5*. Cloning of the disrupted gene in *s327* mutants has identified *radar* as a necessary and sufficient component for dorsal retinal specification.

Along the anterior-posterior axis, this process relies on repellant interactions between ephrin-A ligands and EphA receptors. Chemorepellant interactions alone, however, cannot explain the observed map. It has therefore been suggested that competitive interactions between RGCs cause posterior projection of RGC axons, and are necessary for correct topographic map development. Using larval zebrafish and a novel

experimental paradigm, I have tested the role of proposed axon-axon competition during retinotectal projection, and found that RGC-RGC interactions do not play a significant role in determining distal target location in the retina, but do affect axon arbor morphology by restricting arbor branch number and location.

TABLE OF CONTENTS

List of Figures	vii
Chapter 1 Introduction	1
Figures	5
Chapter 2 The Secreted Morphogen Radar/GDF6a Specifies Dorsoventral Position in the Zebrafish Retina	7
Summary	7
Results, Discussion	8
Methods	15
Figures	19
Acknowledgments	29
Chapter 3 Axon-Axon Interactions Are Required For Arbor Pruning But Not For Formation Of The Retinotectal Map	30
Summary	30
Results/Discussion	31
Methods	37
Figures	40
Acknowledgments	51

Chapter 4	RGC Axon Lamination Does Not Require RGC-RGC Interactions	52
	Results/Discussion	52
	Methods	53
	Figures	54
Chapter 5	Future Directions And Concluding Remark	56
	References	59

LIST OF FIGURES

Figure number	Title	Page
Figure 1.1	Schematic representation of retinotopic mapping along the AP axis.	5
Figure 1.2	Summary of molecular regulation of dorsal-ventral patterning.	6
Figure 2.1	Morphological and retinotectal phenotypes of <i>radar</i> ^{s327} .	19
Figure 2.2	The <i>s327</i> mutation disrupts the <i>radar</i> gene.	21
Figure 2.3	Cell-cell signalling through Radar is sufficient for ventral tectum innervation.	22
Figure 2.4	Radar signalling affects known determinants of dorsal-ventral retinal patterning.	24
Figure 2.5	Reduced eye size in <i>s327</i> mutants is due to increased cell death.	26
Figure 2.6	Dominant-negative inhibition of BMP signalling phenocopies <i>s327</i> .	27
Figure 2.7	Additional analysis of Radar signalling and regulation.	28
Figure 3.1	Two potential mechanisms for formation of the retinotectal map.	40

Figure 3.2	Retinotectal mapping functions in the presence or absence of axon-axon interactions.	41
Figure 3.3	Evidence for normal patterning of retina and tectum in <i>lak</i> mutants.	43
Figure 3.4	Axon-axon competition restricts axon arbor size and complexity.	45
Movie 3.5	RGC axon pathfinding errors during retinal exit in WT ^{<i>Brn3c:mGFP</i>} -> <i>lak</i> chimeras.	47
Figure 3.6	Example quantification of retinal and tectal position in a single chimeric larva.	48
Figure 3.7	Frequency of cell types identified by single cell electroporation in WT and <i>lakritz</i> larvae.	50
Figure 4.1	Single axon laminar choice in WT and <i>lak</i> hosts.	54
Table 4.1	Number of RGC axon arbors terminating in SO and SFGS at 4 and 7dpf.	55

CHAPTER 1

INTRODUCTION

Sensory input to the nervous system relies on the faithful transfer of information from sensory structures to the brain, where input is further processed. A number of sensory systems employ topographic maps to maintain spatial relationships between neighboring presynaptic and postsynaptic cells. Broadly speaking, forming such a map relies on two processes: patterning the originating structure and its target region to establish positional information, and subsequently linking positionally appropriate regions. The following studies describe experiments meant to make progress on both of these broad topics within the zebrafish retinotectal projection.

The retinotectal projection provides a well-characterized example of a topographic map (McLaughlin *et al.* 2003) (Lemke and Reber 2005) (Goodhill 2007). Neighboring retinal ganglion cells (RGCs) in the ganglion cell layer of the retina project axons that arborize on neighboring regions of their midbrain target, the optic tectum in nonmammalian vertebrates or superior colliculus in mammals. More specifically, RGCs in increasingly nasal retinal regions project axons to more posterior tectal targets, while increasingly temporal RGC axons target more anterior regions (Fig. 1.1). Similarly, mapping is maintained along the orthogonal axes. Increasingly dorsal RGCs project to increasingly ventral (lateral) tectal targets. Ventral RGCs project to dorsal (medial) tectum.

Owing to its functional significance and experimental accessibility, a number of findings have provided considerable insight into the processes and molecules responsible for patterning the retina and the development of the retinotectal projection (Lemke and Reber 2005; McLaughlin *et al.* 2003).

To summarize a significant body of work, the neural retina is patterned through spatially restricted expression of genes. Following cues likely established prior to evagination of the optic cup from the developing forebrain, the neural retina, is divided along two axes of importance to retinotectal map formation: the nasal-temporal (or anterior-posterior), and the dorsal-ventral. Altering expression of molecular markers in any of these domains can lead to aberrant retinotectal mapping.

Specifically along the dorsal-ventral axis, a model has emerged which favors BMP family genes as drivers of dorsal specification. Further study of this network of genes and the identification on a new gene required for dorsal specification and appropriate retinotectal mapping is the topic of chapter 2.

Following patterning, classes of retinal neurons are born in temporal waves, starting with the RGCs (Dyer and Cepko 2001). These RGCs later elaborate axons which exit the retina, traverse the midline, and follow the optic tract to the contralateral tectum guided by a number of attractive and repulsive cues. At the tectum, the topographic map is organized. Along the anterior-posterior axis the organization at least partially relies on repulsive EphA/ephrin-A molecular gradients to prescribe locations for axonal arborization. However, the *in vivo* studies responsible for this current understanding have focused largely on gradients and their effects. By their nature, these

studies highlight the roles of RGC position and RGC-external cues while they shroud potential interactions between individual RGCs.

A number of lines of evidence suggest that interactions between RGC axons could affect the development of the retinotectal projection. An older body of literature suggests a rich repertoire of possible axon-axon interactions, such as regionally-selective fasciculation (Bonhoeffer and Huf 1980) and competition for tectal space and synapses (Davis and Schlumpf 1984) (Hayes and Meyer 1988) (Schmidt and Coen 1995). Additionally, more recent results hint at a role for competition among RGC axons in the establishment of the retinotopic map (Reviewed in Wilkinson, 2004). However, to this point, it has not been clear to what extent these cell-cell mechanisms contribute to retinotectal connectivity. Experiments addressing this question will be the focus of chapter 3.

Combined, these experiments shed new light on important processes in retinotectal map formation. They also open further doors for research, some of which will be touched upon in the final chapter.

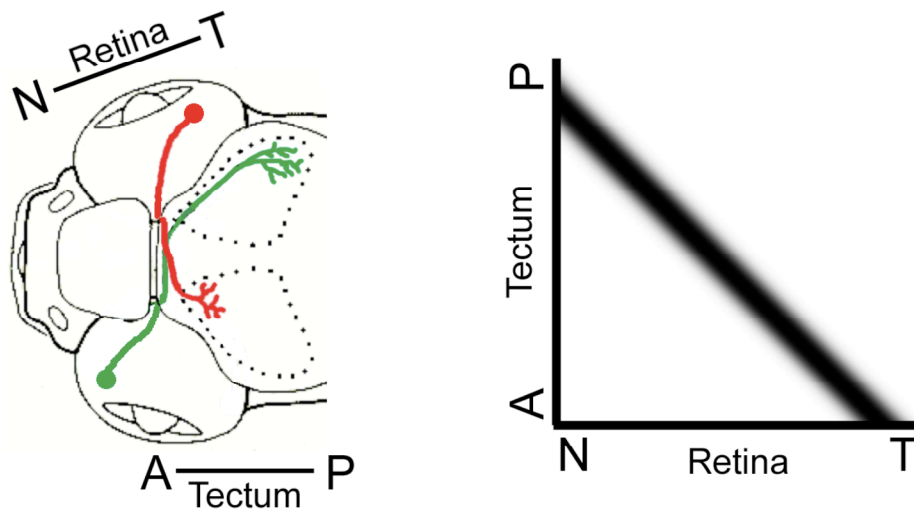
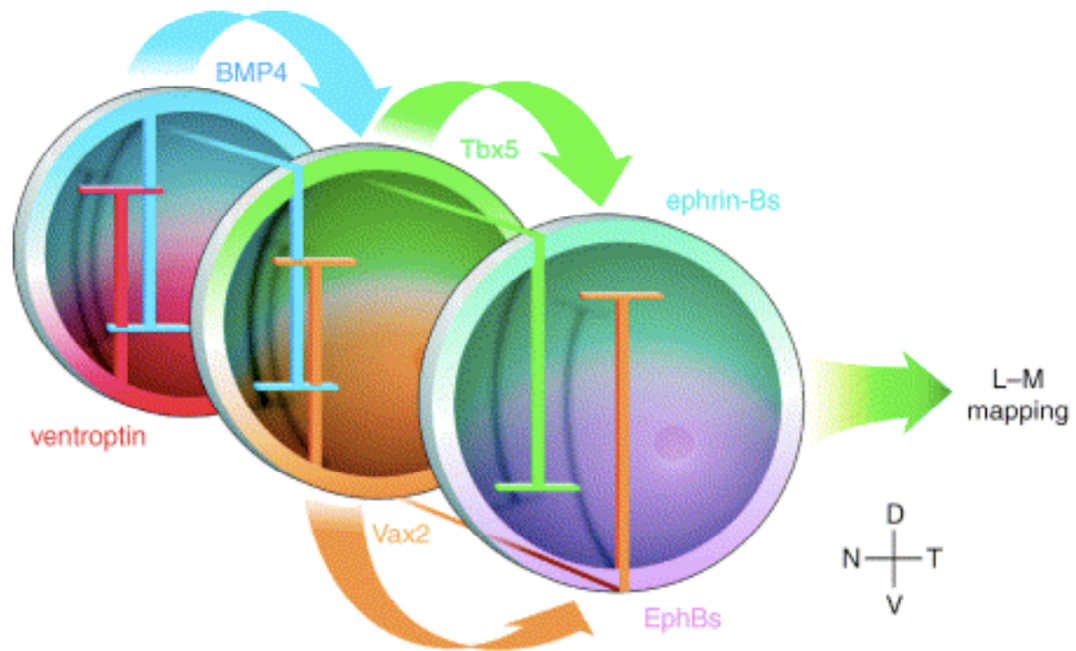


Figure 1.1: Schematic representation of retinotopic mapping along the AP axis.

RGCs in Temporal retina (red) terminate in anterior tectum. Axons from RGCs in more nasal retinal locations terminate in more posterior tectal positions. On the right, an idealized retinotectal mapping function.



Current Opinion in Neurobiology

Figure 1.2: Summary of molecular regulation of dorsal-ventral patterning. Figure reproduced from McLaughlin et al., 2003. A cascade of dorsal and ventral-specific genes, starting with *bmp4* and *ventroptin*, was previously modeled to dictate dorsal and ventral retinal specification, driving retinotectal mapping.

CHAPTER 2:
THE SECRETED MORPHOGEN RADAR/GDF6A SPECIFIES
DORSOVENTRAL POSITION IN THE ZEBRAFISH RETINA

Summary:

The dorsal-ventral and anterior-posterior axes of the retina are specified during embryonic development by signalling mechanisms involving locally secreted factors and asymmetrically expressed transcription factors (Harada *et al.* 2007; McLaughlin *et al.* 2003). These patterning mechanisms provide positional information to retinal ganglion cells (RGCs), which enable their axons to project to the topographically correct target regions in the midbrain tectum. Axons from dorsally located RGCs project to ventral positions in the tectum, while axons of ventral RGCs project to dorsal tectum (Harada *et al.* 2007; McLaughlin *et al.* 2003). This selectivity is achieved by signalling between RGC axons and tectal neurons, which express EphB and ephrin-B molecules in matching gradients along the dorsal-ventral axes of both the retina and the tectum (Hindges *et al.* 2002; Mann *et al.* 2002). Graded positional information is thus used to form a smooth retinotectal map. We show here that the secreted molecule Radar is necessary and sufficient to instruct dorsal retinal fate in zebrafish by activating the expression of dorsal retinal markers and by repressing ventral determinants. Radar misexpression in the ventral retina “dorsalizes” the retinotectal specificity of nearby cells in a cell-nonautonomous manner. Previously identified secreted factors, such as Bmp4, are regulated by Radar and require Radar for signalling, likely through a shared receptor,

Alk8. We suggest that a gradient of Radar specifies dorsal-ventral positional information in the retina.

Results, discussion:

In a large-scale chemical mutagenesis screen for disruptions of the visual system (Muto *et al.* 2005), we discovered a zebrafish mutant with smaller eyes, but otherwise normal external morphology. Despite a transient increase in cell death in the embryonic eye (Supplemental Fig. 2.5), the *s327* mutant retina is laminated normally and supports most visual responses (Muto *et al.* 2005). Noticeably, *s327* mutants are unable to adjust the distribution of melanin pigment in the body to varying levels of ambient light, a retina-dependent, neuroendocrine response termed “visual background adaptation” (VBA) (Kay *et al.* 2001; Neuhauss *et al.* 1999) (Fig. 2.1a). Injection of axon tracer dyes into the eye revealed an abnormal retinotectal projection in *s327* mutants (Muto *et al.* 2005). In wild-type (WT) larvae, the projection zone of RGC axons, as visualized by the *Brn3c:mGFP* transgene (Xiao *et al.* 2005), fills the entire tectal neuropil (Fig. 2.1b). In *s327* mutants, by contrast, retinal axons project to only the dorsal half the tectum (Fig. 2.1b). The ventral half of the tectum, although of normal size and apparently fully differentiated, is devoid of retinal afferents. We asked if dorsal-ventral specificity was still evident within this compressed region of retinal innervation. Axon tracing with the lipophilic dyes DiI and DiO, injected into the dorsal and ventral retina, respectively, showed that, in the half-innervated *s327* tectum, retinotopic order persists (Fig. 2.1c).

Thus, some dorsal-ventral positional information appears to be retained among RGC axons in *s327* mutants.

To identify the genetic lesion responsible for the phenotype, we mapped *s327* to chromosome 16 near marker *z26293* using a panel of 874 recombinant embryos (Knapik *et al.* 1998; Shimoda *et al.* 1999) (Fig. 2.2a). The *radar* gene, encoding the secreted TGF β family member Radar/Gdf6a, represented an excellent candidate for *s327* based on its known expression in the dorsal retina during embryogenesis (Asai-Coakwell *et al.* 2007; Chang and Hemmati-Brivanlou 1999; Rissi *et al.* 1995), and recent implication as a regulator of retinal marker expression (Asai-Coakwell *et al.* 2007). PCR amplification and sequencing of the *radar* cDNA in *s327* mutants and WT siblings revealed a single C-to-A transversion, which introduces a stop codon early in the open reading frame (Fig 2b). The mutant allele is predicted to encode a truncated pro-protein of 54 amino acids, which lacks the putative C-terminal mature signalling peptide characteristic of many TGF β family proteins (Rissi *et al.* 1995) (Fig. 2.2b-c).

Consistent with a role in dorsal-ventral patterning of the embryonic retina, we found *radar* to be expressed in the distal optic vesicle of WT zebrafish embryos as early as the 10-somite stage, with expression maintained in the dorsal retina beyond the 26-somite stage (Fig. 2.2d). In *s327* mutant embryos, *radar* expression is reduced in the optic vesicle at the 10-somite stage and absent in the retina by the 26-somite stage (Fig. 2.2d). This loss of mRNA is likely due to nonsense-mediated decay of the *s327* mutant transcript and further suggests a complete loss of zygotic Radar function in *s327* mutants.

To functionally confirm that *s327* is a loss-of-function allele of *radar*, we sought to rescue dorsal retinal fate by reintroducing WT *radar*. To avoid disrupting early gastrulation and axial patterning events that are dependent on *radar* (Sidi *et al.* 2003), we created a heat-shock inducible *radar* construct (*hsp70:radar^{WT}*). To identify the appropriate time of development for *radar* induction, we employed *hs:dnBMPR* transgenic embryos, in which all Gdf and Bmp signalling is blocked following expression of a dominant-negative receptor (Pyati *et al.* 2005), and found that this signalling pathway is required for dorsal retinal fate at the 12 to 14-somite stage (Fig. 2.6).

Heterozygous *s327* adults carrying *Brn3c:mGFP* were mated and their offspring co-injected with *hsp70:radar^{WT}* DNA and transposase mRNA at the one or two-cell stage. Embryos were then heat-shocked at the 12-somite stage. Injected embryos were raised to 7 days post-fertilization (dpf), and their retinotectal projections investigated. In WT, overexpression of *radar^{WT}* often resulted in embryos with small eyes lacking ventral characteristics (35%, $n > 50$ injected embryos). In these eyes, the optic fissure failed to close, consistent with a loss of ventral retinal identity (Take-uchi *et al.* 2003). This is opposite to uninjected *s327* mutants, in which a duplicated fissure could sometimes be detected in the dorsal retina (see Fig. 2.2d). In *s327* mutants, heatshock-induced expression of *radar^{WT}* restored innervation of the ventral tectum (60%, $n = 20$; Fig. 2.3a-c). Together, these experiments demonstrated that Radar is necessary to specify dorsal retinal identity.

We asked if *radar^{WT}* expression could rescue the visual phenotypes of *s327* mutants. In control clutches from a cross of two heterozygous carriers, VBA-negative

(dark) larvae were found near the expected Mendelian frequency (uninjected with heat shock: 26.7%, $n = 105$; injected without heat shock: 20.3% $n = 69$). Progeny from the same cross injected with *hsp70:radar*^{WT} and heat-shocked at the 12-somite stage showed a significant reduction in the fraction of VBA-negative larvae (2.2%, $n = 92$). Injection and induced expression of the mutant allele found in *s327* mutants (*hsp70:radar*^{s327}) failed to reduce the number of dark larvae (25.4%, $n = 59$). Previous experiments have shown that the retina and optic nerve, but not the tectum, are required for the VBA (Kay *et al.* 2001; Roeser and Baier 2003). Several extratectal, visual areas also lack retinal input in *s327* mutants (Muto *et al.* 2005). Together, our results suggest that a subpopulation of RGCs, projecting to regions outside the tectum, are specified by Radar, and are required for the VBA.

As Gdf6 has previously been shown to be secreted (Chang and Hemmati-Brivanlou 1999), we expected that zebrafish Radar could act on neighbouring cells in a cell-nonautonomous fashion. We therefore tested if WT retinal cells could rescue the *s327* mutant retinotectal projection phenotype by transplanting cells at the blastula stage from WT donors to *s327* mutant hosts. The hosts carried the *Brn3c:mGFP* transgene. In these chimeras ($n = 41$), which were selected at 30 hpf for the presence of donor cells in the retina, we observed a number of genotypically mutant host (GFP-labeled) axons in the ventral tectum (Fig. 2.3d), demonstrating that Radar acts non-autonomously to instruct, or permit, a dorsal fate.

We then asked if Radar overexpression was sufficient to cause ventrally located RGCs in WT to gain a dorsal identity. Because embryo-wide overexpression of *radar*

prevented innervation of the tectum, we injected WT embryos with *hsp70:radar^{WT}*. We then transplanted blastomeres from this *hsp70:radar^{WT}* mosaic embryo into a WT host. The resulting chimeras, were heat-shocked at the 12-somite stage to induce *radar* expression, sorted for the presence of donor-derived cells in the retina, and allowed to develop. At 7 dpf, DiO was injected at the ventral margin of the retina to label the retinotectal projection. Whereas in all non-heatshocked controls ($n = 10$), DiO-labeled axons projected exclusively to the dorsal tectum (Fig. 2.3e), in all heatshocked chimeras ($n = 3$), some axons were seen terminating in the ventral tectum (Fig. 2.3f). These data suggest that Radar acts on neighboring cells and that it can override ventral fate determining factors.

In the developing optic vesicle of chicken, secreted BMP factors stimulate *tbx5* expression, which is required for dorsal repression of *vax2* (Barbieri *et al.* 1999; Mui *et al.* 2002) and dorsal activation of *efnb2* (Koshiba-Takeuchi *et al.* 2000; Sakuta *et al.* 2006). Altered expression of these factors leads to abnormal retinotectal mapping (Koshiba-Takeuchi *et al.* 2000; McLaughlin *et al.* 2003; Schulte *et al.* 1999). To determine if this patterning system is dependent on Radar function, we performed *in situ* hybridizations. In WT retinas at the 26-somite stage, expression of *bmp2b*, *bmp4* and *tbx5* are restricted to the dorsal retina, opposite the optic fissure (Fig. 2.4a-c), while *vax2* is restricted to the ventral retina (Fig. 2.4d). In *s327* mutants, *bmp2b* expression appears largely unaffected, but *bmp4* and *tbx5* expression are substantially reduced or absent (Fig. 2.4f-h). Additionally, the *vax2* expression domain is expanded (Fig. 2.4i). Conversely, *radar* overexpression with *hsp70:radar^{WT}* has only slight effects on *bmp2b* (observed in 66% of the injected embryos), but induces ectopic *bmp4* and *tbx5* and completely abolishes *vax2*

in almost all embryos ($n > 10$ for each experiment; Fig. 2.4k-n). The *tbx5* domain often fills the entire retina in *radar* overexpressors (57% of injected embryos, $n = 21$; Fig. 2.4m).

Similar to *s327*, we observed a reduction of *tbx5* expression in zygotic *lost-a-fin* mutants (Fig. 2.7a, b), in which the type I Bmp receptor Alk8 is disrupted (Mintzer *et al.* 2001). This suggests that Alk8 acts as one of the receptors for Radar in retinal patterning, as it does in earlier axial patterning of the embryo (Goutel *et al.* 2000; Sidi *et al.* 2003). Although recent studies have speculated on a role for Radar in nasotemporal specification based on morpholino-mediated knockdown¹², we did not observe significant differences between expression patterns of the temporal marker *epha4b* in WT, mutant, and *hsp70:radar^{WT}* overexpressing embryos (Fig. 2.4e, j, o).

Bmp2b and Bmp4 are expressed in the dorsal retina of zebrafish (see Fig. 2.4a, b), and each can expand the *tbx5* domain and suppress *vax2* when overexpressed in chick (Koshiba-Takeuchi *et al.* 2000), similar to Radar (see Fig. 2.4m, n). We reported above that the *bmp2b* gene is slightly and the *bmp4* gene substantially upregulated by *radar* (see Fig. 2.4f, g, k, l). We were interested if this interdependence is reciprocal. As in chick, *tbx5* is expanded and *vax2* is repressed following heatshock-induced overexpression of *bmp4* (Fig. 2.4q, r) or *bmp2b* in WT (Fig. 2.7f, g). The expression of *radar*, however, appears unchanged by either treatment (Fig. 2.4p; Fig. 2.7e). In *s327* mutants, *bmp4* overexpression is unable to fully expand *tbx5* ($n = 23$) and fails to reduce the dorsal expansion of *vax2* ($n = 9$) (Fig. 2.4t, u). Furthermore, morpholino-mediated knockdown of either *bmp2b* (Imai and Talbot 2001) or *bmp4* (Shin *et al.* 2007) fails to

prevent expression of either *radar* or *tbx5* expression in the eye (not shown). Together, these data indicate that *radar* is not regulated by either *bmp2b* or *bmp4* and that dorsalization of the retina by *bmp4* requires functional *radar*.

While a network of TGF β factors specify dorsal retinal fate, hedgehog factors, such as Shh, appear to act in a countergradient to instruct ventral characteristics (Take-uchi *et al.* 2003). Shh is not expressed in the eye, while the dorsoventral axis is laid down, but rather secreted from the midline of the neural tube (Take-uchi *et al.* 2003). We found that *radar* expression is slightly, if at all, expanded in the retinas of zebrafish *syu* mutants, which lack Shh (Schauerte *et al.* 1998) (Supplemental Fig. 2.7), and expression of the Shh target *ptc1* is unaltered in *s327* mutants (not shown). Together, this suggests that the Radar gradient is present in the absence of Shh. Residual dorsal-ventral information seen in *s327* mutants (see Fig. 2.1c) may thus be conveyed either by Shh (Take-uchi *et al.* 2003; Zhang and Yang 2001) or by Radar-independent Bmp signalling (Behesti *et al.* 2006).

Our new data, combined with previous studies (Harada *et al.* 2007; McLaughlin *et al.* 2003), suggest a model that assigns *radar* a central function in the gene network that specifies dorsal retinal identity (Fig. 2.4p). We propose that the *radar* gene product, potentially by dimerizing with other Bmps (Chang and Hemmati-Brivanlou 1999), such as Bmp2b and later Bmp4, and by signalling through Alk8, is required to establish a retinal gradient of *tbx5*. The product of *tbx5* promotes dorsal retinal fate, including expression of axon guidance factors, such as Efnb2, and inhibits ventral retinal fate by repression of

vax2(Koshiba-Takeuchi *et al.* 2000). Our studies have thus identified an important determinant of retinal positional information.

Methods

Strains and Maintenance. Fish were maintained as previously described(Muto *et al.* 2005).

Immunohistochemistry. Larvae were raised in with 0.003% (w/v) 1-phenyl-2-thiourea (PTU) to inhibit melanin synthesis. Whole-mount TUNEL staining and immunohistochemistry were performed as described elsewhere(Wehman *et al.* 2005), using antibodies *zrf-3* (Oregon monoclonal bank) diluted 1:250, and anti-GFP (Molecular Probes) diluted 1:1000.

Fluorescent axon tracing. Dye injections were performed as previously described(Muto *et al.* 2005).

Confocal microscopy. Live larvae were mounted in 1% low melting point agarose in E3 medium and treated with 0.8% norepinephrine to aggregate melanin pigment granules and anaesthetized with 0.016% tricaine. Fixed larvae were mounted in 1.6% low melting point agarose in PBS. Confocal imaging was performed with long-working distance lenses (20X, NA 0.5; 40X, NA 0.8) on a Zeiss Pascal confocal microscope. Images were analyzed and processed with ImageJ and Adobe Photoshop.

Positional cloning and RFLP analysis. Linkage mapping was performed as described(Muto *et al.* 2005). First strand cDNA was synthesized from 8 dpf homozygous

s327 mutants, WT siblings, and homozygous TL (WT strain) larval zebrafish. The *radar* open reading frame (ORF) was amplified by PCR using specific primer sequences (forward 5'-ATGGATGCCTTGAGAGCAGTC-3' and reverse 5'-CTACCTGCAGCCACACTGTTC-3'). The *s327* mutation destroys an SfaNI site, allowing identification of carriers by restriction fragment length polymorphism (RFLP) analysis. Amplification from genomic DNA by PCR with the forward primer and the RFLP reverse primer (5'-TTGAAGAGCGGAAAAAGCTC-3'), followed by digestion with SfaNI resulted in products of 170 and 110 bp in WT, and a single band of 280 bp from *s327* mutants.

***In situ* hybridization.** Dig-labeled riboprobes for full-length *radar*, *tbx5*, *bmp2b* and *vax2* were transcribed *in vitro*. *s327* mutants and WT siblings were stained as a clutch, with expected mutant frequencies of 25%. *laf* and *syu* mutants were identified prior to staining, then treated with identical conditions. Whole-mount *in situ* hybridizations were carried out as previously described (Kay *et al.* 2005) and stored in 87% glycerol. Eyes were dissected using tungsten needles and mounted in a similar orientation. For *bmp4*, *tbx5* and *vax2*-stained embryos lacking staining in the retina, eyes were dissected from animals that had comparable levels of staining in other tissues. All images were collected with a Leica dissection microscope or a Zeiss compound microscope equipped with a Spot CCD camera (Diagnostic Instruments), and prepared using Adobe Photoshop.

s327 mutant and WT sibling embryos were genotyped by RFLP analysis (see above), with DNA isolated prior to imaging by clipping the trunk, or following imaging using the entire embryo. DNA was isolated by methanol dehydration, tissue maceration and

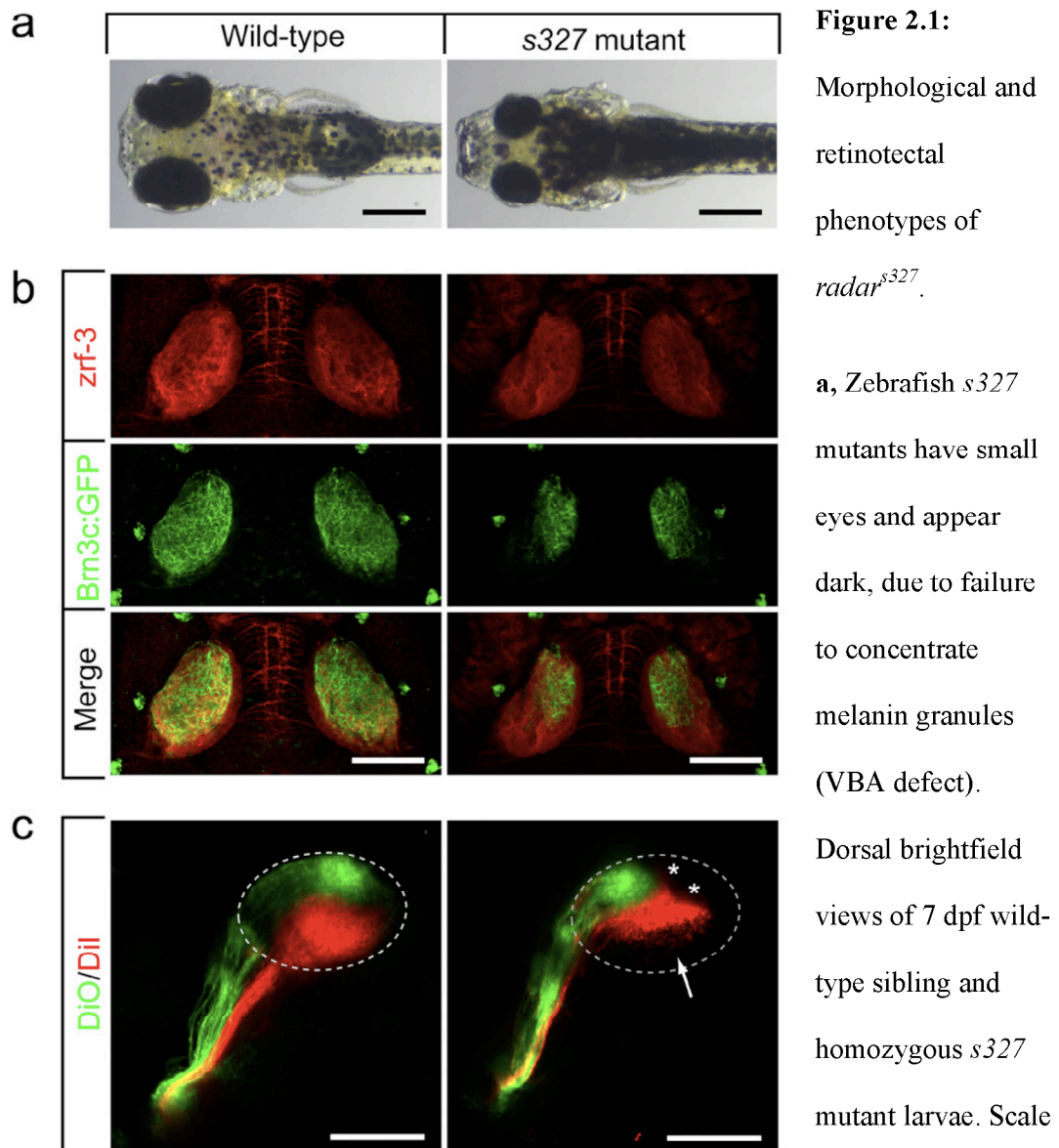
overnight incubation in 1.7mg/μL proteinase-K (Roche) in 10mM Tris, pH 8.0. Images shown are representative of respective genotypes.

Injection and heatshock induction. The *radar* ORF was amplified with modified forward and reverse cloning primers (see above) containing Sall restriction sites, and subcloned downstream of the *hsp70* promoter in a construct flanked by Tol2 transposase recognition sites(Scott *et al.* 2007).

For all rescue experiments, 10 ng/μL DNA was coinjected with 25 ng/μL Tol2 transposase mRNA, and 25 ng/μL GFP mRNA generated with the mMessage mMachine kit (Ambion) at the 1-2 cell stage. Poorly injected (identified by a lack of strong GFP fluorescence) and malformed embryos were excluded from the experiment prior to heatshock. All heatshock inductions were accomplished as described(Pyati *et al.* 2005).

VBA analysis of injected larvae was performed blind to injected status as described(Muto *et al.* 2005). The *bmp4* ORF was amplified by PCR and Xi cloned (Gene Technology Systems, San Diego) into a vector containing 14 repeats of the upstream activating sequence (UAS), and flanked by Tol2 sequences(Scott *et al.* 2007). 10 ng/μL DNA was injected into an incross of carriers of the *s327* mutation and the *hsp70:gal4* transgene. Heatshock induction was carried out at 12 somites to allow sufficient time for Gal4-mediated transactivation. Similar injection controls were done, and only animals with increased trunk and tail thickness indicative of BMP overexpression were kept for staining. Heat-shock induced overexpression of *bmp2b* was similarly achieved using transgenic embryos(Shin *et al.* 2007).

Transplantation experiments. Donor embryos were injected with a solution of 1-5% tetramethyl-rhodamine dextran amine (Molecular Probes). Blastula-stage transplants were performed as described (Kay *et al.* 2005). Chimeras were sorted at 30-36 hpf for the presence of rhodamine-positive cells in the neural retina and treated with PTU. For overexpressing chimera experiments, donors were also coinjected with 25 ng/ μ L *hsp70:radar^{WT}*, 25 ng/ μ L Tol2 transposase mRNA, and 25 ng/ μ L GFP mRNA. Following heatshock at 12 somites, chimeras were sorted and treated as above.

**Figure 2.1:**

Morphological and retinotectal phenotypes of *radar*^{s327}.

a, Zebrafish *s327* mutants have small eyes and appear dark, due to failure to concentrate melanin granules (VBA defect).

Dorsal brightfield views of 7 dpf wild-type sibling and homozygous *s327* mutant larvae. Scale

bar is 300 μ m. **b**, *s327* mutants lack ventral innervation of the optic tectum. Dorsal confocal projections of 7 dpf larvae show that innervating RGC axons (visualized by *Brn3c:mGFP*) are confined to the dorsal tectum in mutant larvae. Co-staining with a neuropil marker (*zrf-3* antibody) show similar tectal architectures in WT and mutants. **c**, *s327* mutants have a compressed dorsal-ventral retinotectal map. Fixed WT and *dar1*^{s327} larvae eyes (7 dpf) were injected with DiO (ventrally) and Dil (dorsally). Lateral confocal

projections are shown. Arrow highlights region not innervated by RGCs in *s327*;
asterisks show positions of skin melanophores. Scale bar is 300 μm in **a**, 100 μm in **b**, **c**.

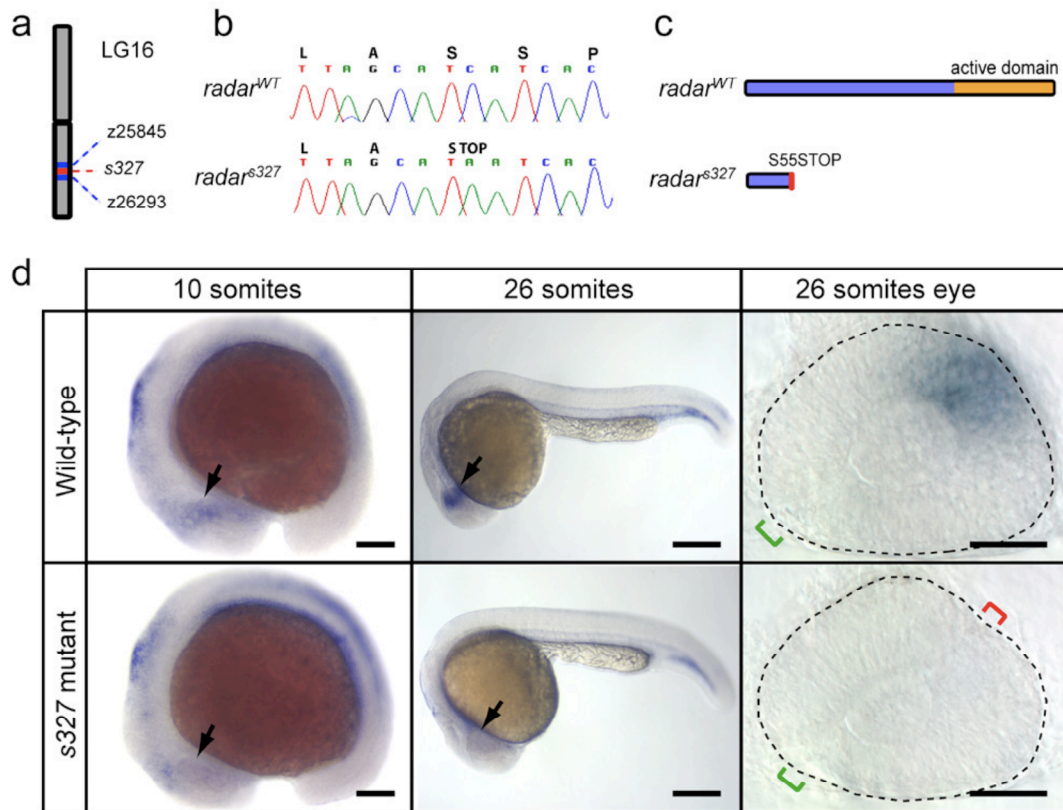


Figure 2.2: The *s327* mutation disrupts the *radar* gene.

a, *s327* maps to chromosome 16. **b**, Sequencing of WT and *s327* cDNA reveals a single C-to-A substitution in position 164 of the *radar* ORF, resulting in a premature stop codon. **c**, Predicted translated peptides arising from *radar*^{WT} and *radar*^{s327}. The mutation results in a truncated peptide, lacking the mature signalling domain. **c**, Whole-mount *in situ* hybridization shows a restricted pattern of *radar* expression in WT embryos. *radar* mRNA is largely absent from *s327* mutants at all stages. In WT, expression is evident in the distal optic vesicle of WT embryos at 10 somites (arrow). At 26 somites, *radar* is expressed dorsally, opposite of the optic fissure (green bracket). Note ectopic fissures (red bracket) in *s327* mutants. Scale bars are 150 μ m for 10 somites, 250 μ m for 26 somites, 50 μ m for dissected 26 somite eyes.

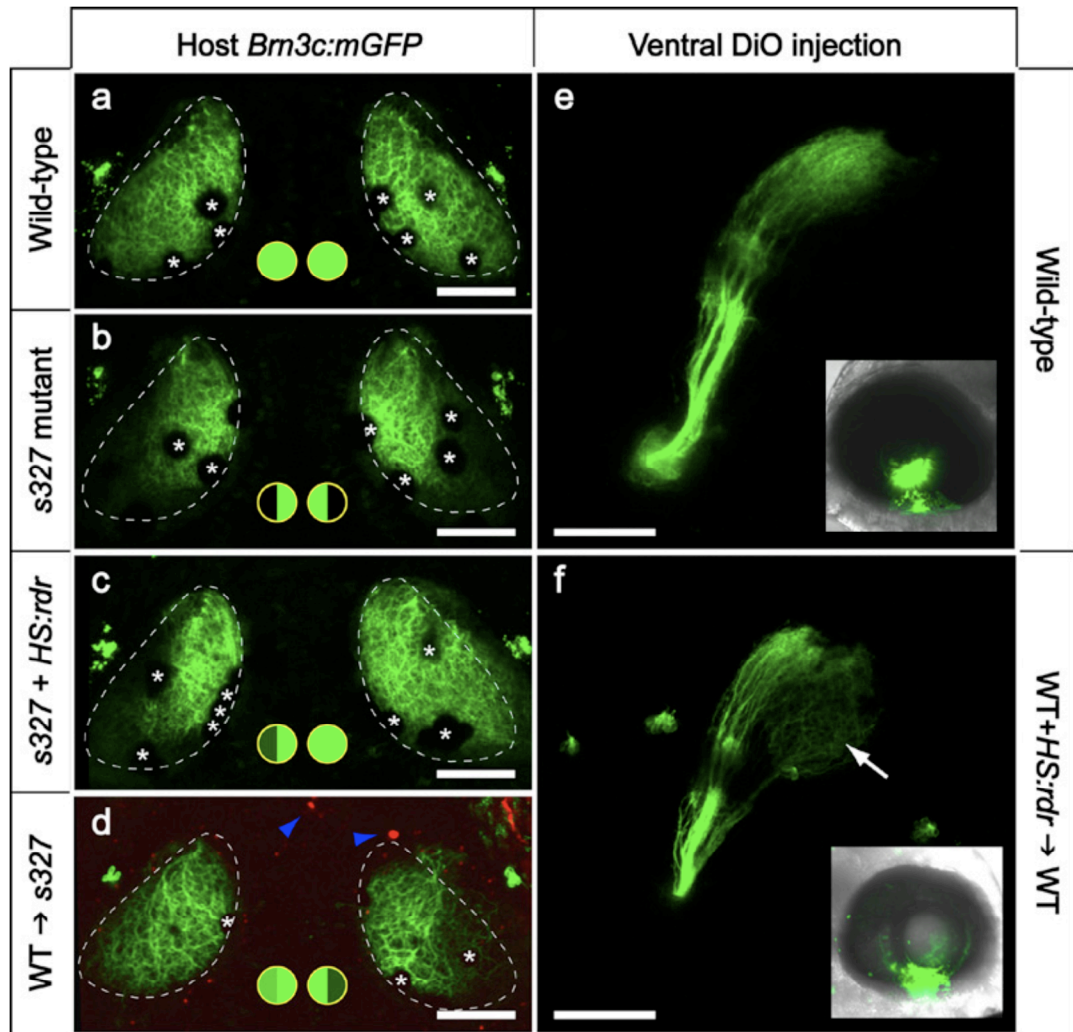


Figure 2.3: Cell-cell signalling through Radar is sufficient for ventral tectum innervation

a-d, Rescue experiment. *Bm3c:mGFP*-labeled retinotectal projections were imaged in vivo at 7 dpf. The tectal neuropil is outlined with a dashed line. Green-filled circles summarize dorsal and ventral tectum innervation results. **a**, WT tecta show full innervation. **b**, *s327* mutants lack ventral innervation. **c**, *radar*^{WT} expression from heatshock-promoter rescues the retinotectal phenotype. Interestingly, in the case shown, only one side was rescued. PCR-based genotyping confirmed that only the rescued eye contained *hsp70:radar*^{WT}; the other eye had likely not received the injected plasmid due

to the mosaicism inherent in transient transgenesis. **d**, The *radar* gene acts cell-nonautonomously in retinal cells. WT cells transplanted into *s327* host embryos are sufficient to rescue ventral innervation. Only the host carried the *Brn3c:mGFP* transgene. Donor-derived cells (blue arrowheads) were labelled with rhodamine-dextran, and do not contribute to the tectum. **e, f**, Gain-of-function experiment. DiO was injected into the ventral retina, and its labelling pattern was imaged from a lateral view. Insets show injected eye. **e**, In normal WT larvae, ventral RGCs project exclusively to the dorsal tectum. **f**, In chimeric WT larvae that have received a transplant of WT cells carrying the *hsp70:radar^{WT}* construct, some ventral axons ectopically innervate the ventral tectum. (arrow). Asterisks (in a-d) show positions of skin melanophores. Scale bars are 100 μm .

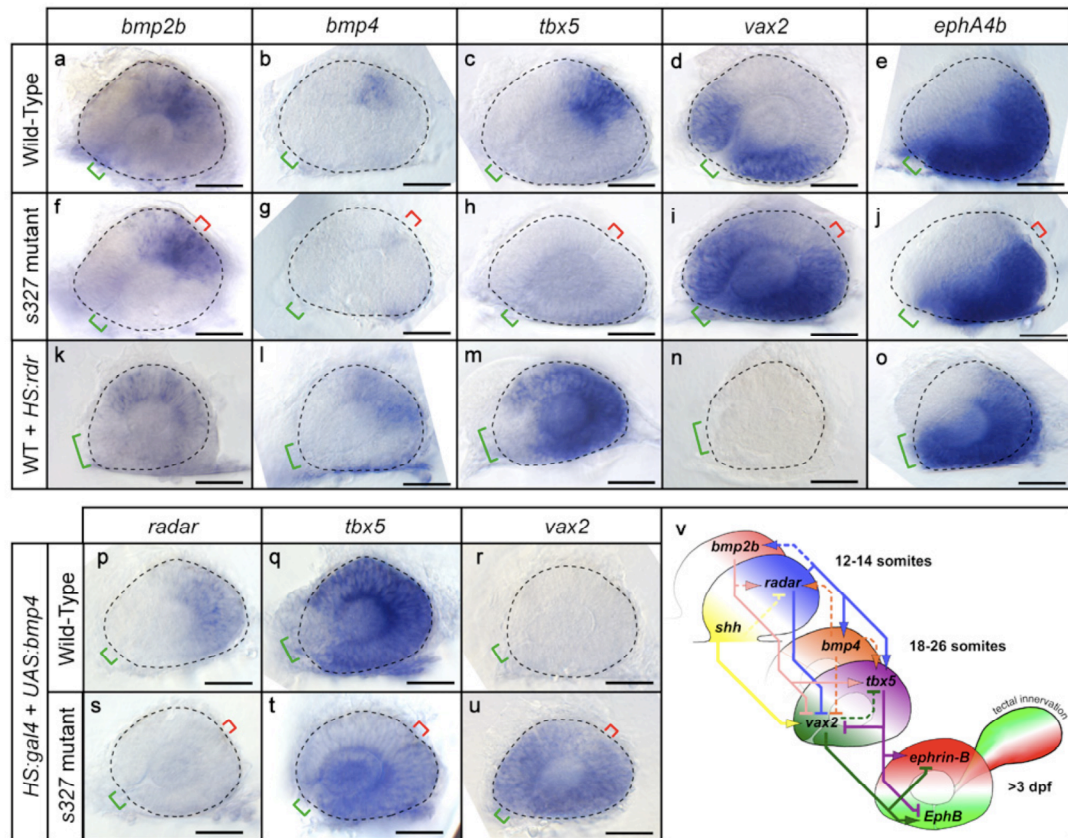
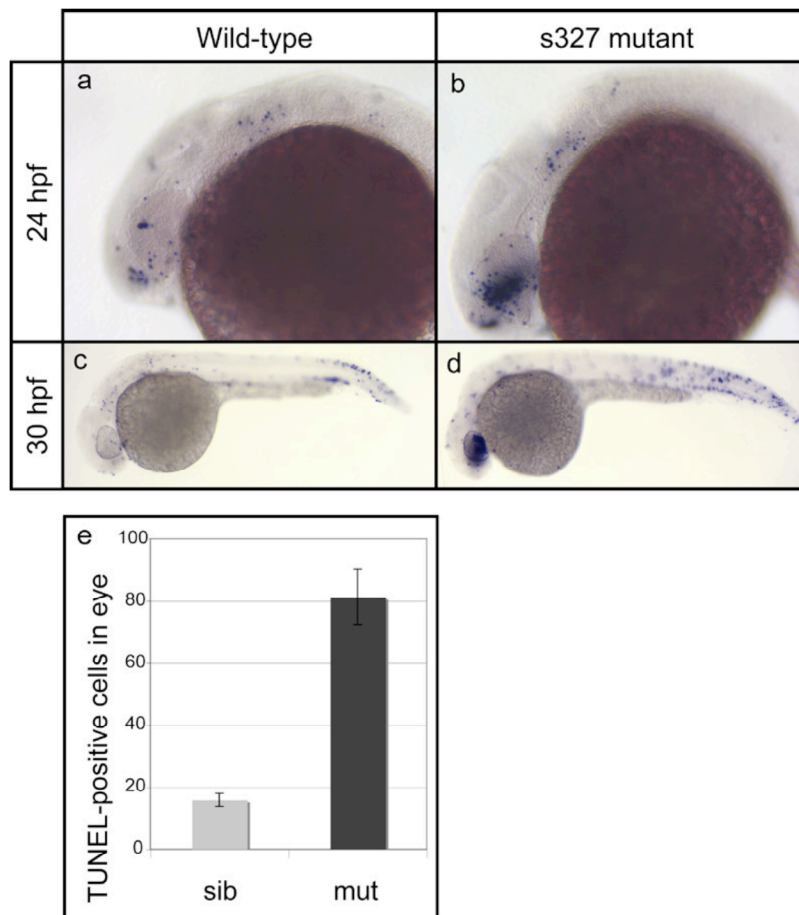


Figure 2.4: Radar signalling affects known determinants of dorsal-ventral retinal patterning.

a-u, Expression patterns visualized by whole-mount *in situ* hybridization of eyes from 26-somite embryos. Neural retina is outlined with dashed line; green bracket identifies optic fissure location and size; red bracket indicates ectopic fissures in mutants. Scale bars are 50 μ m. Expression patterns of known dorsal markers *bmp2b*, *bmp4*, and *tbx5*, ventral marker *vax2*, and temporal marker *ephA4b* in WT (a-e), *s327* mutants (f-j), and WT overexpressing *hsp70:radar^{WT}* (k-o). In *s327* mutants, retinal *bmp2b* expression remained normal, *bmp4* expression was severely reduced, *tbx5* expression was absent, and *vax2* expression was expanded dorsally. In *radar*-overexpressing embryos, *bmp2b*, *bmp4*, and *tbx5* expression were expanded ventrally, and *vax2* was lost. Eyes

overexpressing *radar* were often small and failed to close at the optic fissure. **p-u**, Overexpression of *bmp4* requires *radar* to alter dorsal-ventral patterning. *radar* expression is mildly expanded (p), *tbx5* expression dramatically increases (q), and *vax2* expression is eliminated in WT; *hsp70:gal4; UAS:bmp4* embryos. *radar* expression remains absent (r), *tbx5* is expressed at low levels in ectopic locations (s), and *vax2* expression is dorsally expanded (t) in *s327* mutant; *hsp70:gal4; UAS:bmp4* embryos. **v**, Genetic interaction model, synthesizing roles for Radar with known dorsal-ventral patterning genes. Pointed arrowheads indicate positive influence on RNA expression. Bar arrowheads indicate negative influence. Solid lines indicate relationships supported by both gain-of-function and gene-specific loss-of-function evidence. Dashed lines indicate support from evidence from either gain-of-function or loss-of-function. Largely independent patterning mechanisms establish *radar* and *bmp2b* expression in the distal optic vesicle. Radar is necessary and sufficient to drive expression of *bmp4* and *tbx5* and to repress *vax2* and weakly sufficient to drive ectopic expression of *bmp2b*. Neither Bmp2b nor Bmp4 are necessary or sufficient to drive *radar* expression.

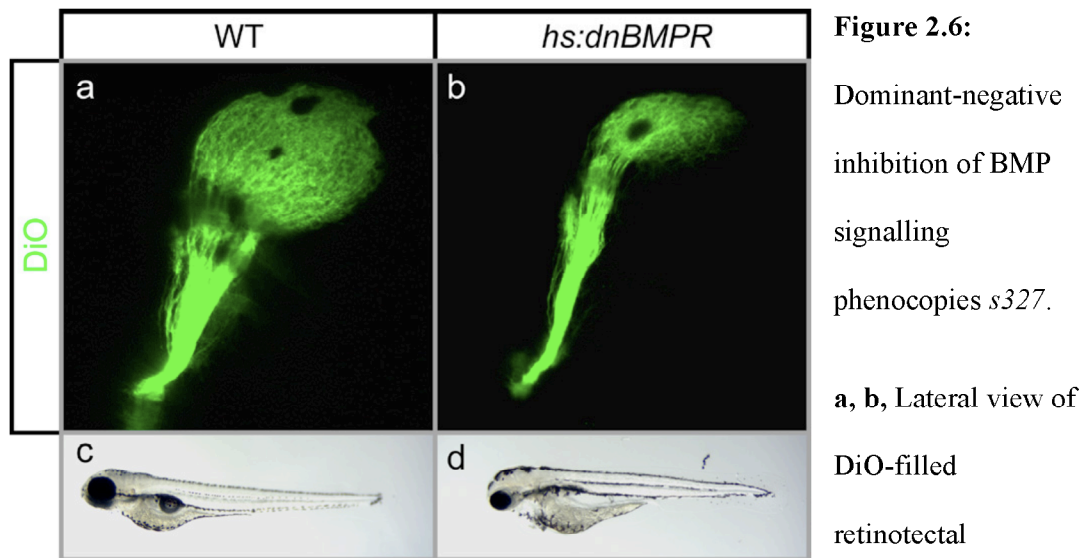
**Figure 2.5:**

Reduced eye size in *s327* mutants is due to increased cell death.

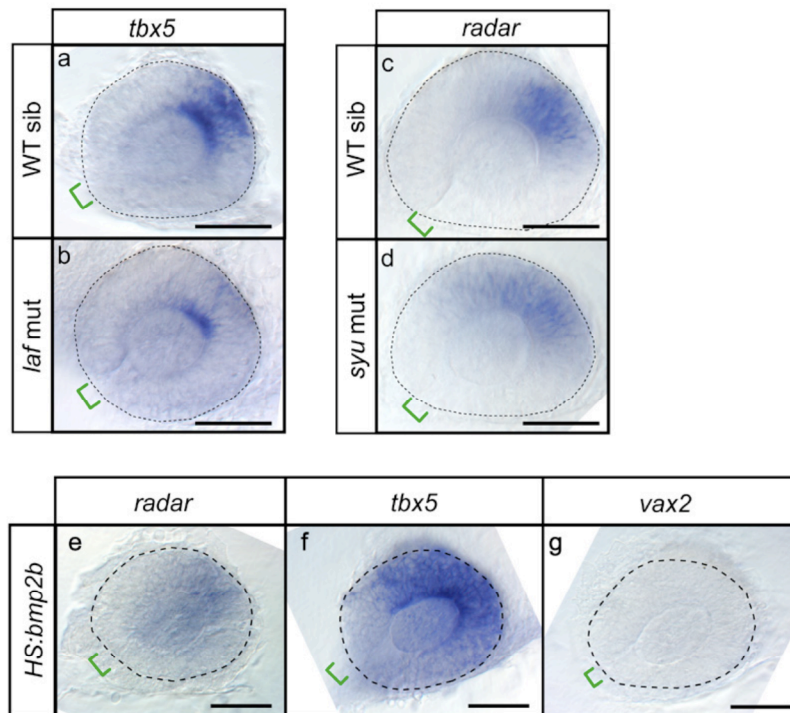
Lateral views of whole-mount

TUNEL-stained embryos. **a**, 24 hpf WT embryos have small numbers of TUNEL-positive cells throughout the

head and trunk. **b**, 24 hpf *s327* mutant embryos have a large increase in TUNEL reactivity in the developing eye. **c**, **d**, 30 hpf *s327* mutant embryos have significantly more TUNEL-positive cells in the eyes than WT. The difference is less dramatic in the trunk. **e**, Quantification of TUNEL staining in 30 hpf embryos. *s327* mutants (n=6) have significantly more TUNEL-positive cells in the eye than WT embryos (n=8, *t*-test, $p < 0.000001$).



projections in 5 dpf larvae heatshocked at 12 somites. **a**, In WT, the entire tectum is innervated. **b**, In *hs:dnBMPR* transgenic animals only dorsal tectum is innervated, similar to *s327*. **c, d**, Brightfield lateral view of 4 dpf larvae. WT larvae (**c**) show normal eye size, while *hs:dnBMPR* larvae (**d**) have smaller eyes similar to *s327*.

**Figure 2.7:**

Additional analysis of Radar signalling and regulation.

a-g, Dissected eyes following whole-mount *in situ*

hybridizations on 26-somite embryos with the antisense probes indicated.

Scale bars are 50 μ m. **a**, WT eyes express *tbx5* in the dorsal retina, opposite of the optic fissure. **b**, *lost-a-fin* (*laf*) mutants, lacking functional Alk8 receptor, have reduced expression of *tbx5*. **c**, In WT eyes *radar* expression is restricted to a narrow patch opposite of the optic fissure. **d**, In *sonic you* (*syu*) mutants, in which Shh is disrupted, *radar* expression is slightly expanded to the ventral retina. **e-g**, *bmp2b* overexpression mirrors the effects of *bmp4* overexpression. *hsp70:bmp2b* transgenic fish were induced at 12-14 somites to overexpress *bmp2b*. *radar* expression is weakly expanded, *tbx5* expression is strongly upregulated, *vax2* expression is absent from the retina.

Acknowledgments We thank Didier Stainier (UCSF), Alexander Picker (MPI Dresden), Mary Mullins (University of Pennsylvania), and the Zebrafish International Resource Center (Eugene) for reagents and fish strains, Julie Pinkston-Gosse and members of the Baier Lab for review of the manuscript.

CHAPTER 3

AXON-AXON INTERACTIONS ARE REQUIRED FOR ARBOR PRUNING BUT NOT FOR FORMATION OF THE RETINOTECTAL MAP

Summary:

The retinotectal projection has long served as an experimental and theoretical paradigm for the study of topographic brain maps (Goodhill 2007; Lemke and Reber 2005; Ruthazer and Cline 2004). Neighboring retinal ganglion cells (RGCs) project their axons to neighboring positions in the optic tectum, thus re-establishing a continuous representation of visual space in their midbrain target. Mapping along this axis requires chemorepellent signaling from tectal cells, expressing ephrin-A ligands, to retinal growth cones, expressing EphA receptors (Flanagan 2006). High levels of ephrin-A, increasing from anterior to posterior, prevent temporal axons from invading the posterior tectum. But the force that drives nasal axons to extend past the anterior tectum and terminate in posterior regions remains to be identified. Here we tested if axon-axon interactions, such as competition, are required for posterior tectum innervation. By transplanting blastomeres from a wild-type (WT) zebrafish into a *lakritz* (*lak*) mutant, which lacks all RGCs (Kay *et al.* 2001), we created chimeras with eyes that contained single RGCs. These solitary RGCs often extended axons into the tectum, where they branched to form a terminal arbor. We show that the distal tips of these arbors were positioned at retinotopically appropriate positions, ruling out an essential role for competition in innervation of the ephrin-A-rich posterior tectum. However, solitary arbors were larger and more complex

than under normal, crowded conditions, due to a lack of pruning of proximal branches during refinement of the retinotectal projection. We conclude that dense innervation is not required for smooth mapping of retinal axons within the tectum, but serves to restrict arbor size and shape.

Results, discussion:

Axons originating in the temporal retina form connections with the anterior (rostral) part of the tectum, whereas nasally located RGCs project to posterior (caudal) tectum (Fig. 3.1a). While a single gradient of repulsive ephrin-A (Fig. 3.1b) is sufficient to explain the projection of temporal axons to anterior tectum, the preference of nasal axons for posterior tectum, where ephrin-As are most highly concentrated, has remained enigmatic. Nasal axons carry fewer EphA receptors and are less sensitive to ephrin-A (Carvalho *et al.* 2006; Hornberger *et al.* 1999), but still avoid high concentrations of ephrin-A *in vitro* (Monschau *et al.* 1997). Therefore, our current understanding of retinotectal mapping relies on a postulated second gradient of activity. In principle, such a gradient could either be presented by the target, independent of axonal input, or be produced by interactions between axons.

To distinguish between these possibilities it is useful to consider the case of a single axon terminating in the tectum in the absence of all other axons (Fig. 3.1c,d). If the map is formed by one-to-one matching of retinal and tectal markers (chemoaffinity) (Gierer 1983; Sperry 1963) then the projection of this solitary axon should be indistinguishable from that of an axon originating from the same retinal position under normal, crowded

conditions (Fig. 3.1c). If, alternatively, interactions between RGC axons are responsible for the production of a second, posterior-directing activity, then retinotopy should be altered when no other axons are present (Fig. 3.1d shows one possible outcome). Recent studies have proposed that individual axons determine their spatial order by comparing their own ephrin-A/EphA signaling levels with that of their neighbors or with that of all other axons (Honda 2003; Reber *et al.* 2004; Tsigankov and Koulakov 2006; Yates *et al.* 2004). These models have been tremendously successful in explaining the plasticity of the map in response to surgical and genetic manipulations (Goodhill and Xu 2005; Lemke and Reber 2005), although pure chemoaffinity theories have also mastered this task (Willshaw 2006). Competition for limiting supply of target-derived factors (e. g., neurotrophins) has been proposed as a cellular mechanism to spread retinal input over the available tectal territory (Fraser and Perkel 1990; Goodhill and Xu 2005; Yates *et al.* 2004). If competition is the force driving nasal axons into repellent territory, then in the absence of other axons, a single nasal axon should always prefer to terminate in the anterior tectum (Fig. 3.1d).

We have now tested this prediction by creating mosaic zebrafish eyes with just one RGC. Cells were transplanted at the blastula stage from WT donors into *lak* mutant host embryos (Fig. 3.2a). *lak* mutants fail to develop any RGCs due to disruption of the proneural transcription factor *Ath5* (*Atoh7*) (Kay *et al.* 2001). WT cells in the mutant environment may undergo the full RGC differentiation program (Kay *et al.* 2005; Poggi *et al.* 2005). The *lak* mutant has no known defects outside of the retina and *ath5* mRNA is only found in the retina. To visualize single RGCs and their axons, WT donor embryos carried the *Brn3c:mGFP* transgene, which is expressed in roughly half of RGCs

projecting to the tectum(Xiao *et al.* 2005). We then selected for analysis those chimeras in which single GFP-labeled axons were resolvable in the tectum.

In chimeras consisting of a WT host which had received cells from a WT donor (WT^{Brn3c:mGFP}->WT; *n*=30 axons), donor-derived, GFP-labeled RGCs exhibited stereotyped retinotectal projections (Fig. 3.2b). Their axons exited the retina, crossed the midline, and innervated the contralateral optic tectum, forming a branched terminal arbor. Remarkably, in *lak* hosts (WT^{Brn3c:mGFP}->*lak*; *n*=19 axons), solitary axons remained capable of the multiple pathfinding steps required for innervation of the contralateral tectum (Fig. 3.2c). Many of these axons projected well beyond the anterior tectum. A minority of solitary RGCs showed pathfinding errors within the retina not seen under normal conditions, when their cell body was in a peripheral region, at a distance from the optic fissure (Supp. Video S1). Our results clearly show that RGC-RGC interactions are not absolutely required for innervation of the posterior tectum.

To analyze possible changes in retinotopy, we compiled summary mapping functions at 7 days post-fertilization (dpf) for single axons that had developed under either crowded or solitary conditions. To this end, we determined the locations of the RGC soma along the nasal-temporal axis in the retina and its axonal arbor in the tectum (see Suppl. Fig. 3.S2 for an example of such an analysis). In WT zebrafish, axons enter the tectum at its anterior pole, extend only in a posterior direction, and do not overshoot their target²⁹. Because single terminal arbors in larval zebrafish cover approximately 5-10% of the tectal surface(Hua *et al.* 2005; Smear *et al.* 2007), we derived two separate

mapping functions per experimental condition: one for the most distal branch, the other for the most proximal branch of each arbor.

As predicted by earlier axon tracing studies in zebrafish (Baier *et al.* 1996; Stuermer 1988), crowded axons form a continuous map. Both distal and proximal branch positions conform to approximately linear and parallel mapping functions (Fig. 3.2d, e). A very similar relationship is seen for the distal branches in solitary axons (Fig. 3.2d). In fact, slope and absolute values of the mapping function are indistinguishable from the crowded condition (F-test, $p=0.630$). A strong difference, however, is seen for the proximal branches (Fig. 3.2e; F-test, $p<0.00001$). Although retinotopic order is retained, the slope of the mapping function is shallower, indicating that solitary axons form (or maintain) branches more anteriorly than crowded axons and that this shift is more pronounced for the nasal axons than for temporal axons.

We asked if the observed anterior shift in proximal branching could be caused by altered retinal or tectal positional cues. Consistent with normal nasal-temporal patterning of the retina, expression of EphA4b, a marker for temporal retina, was unchanged in the *lak* retina (Fig. 3.3a, b). Furthermore, the gradient of ephrin-A5b is maintained in the tectum of *lak* mutants (Fig. 3.3c, d), suggesting that tectal guidance cues are unaffected by the absence of retinal innervation.

Although molecular patterning appears normal in *lak* mutants, it was possible that retinal input might be necessary for tectal cell differentiation or maturation. By imaging individual tectal cells labeled with membrane-bound GFP (see Methods), we found morphologically normal neuronal and glial-like cells in the *lak* mutant tectum (Fig. 3.3c-

h). Additionally, a quantitative survey revealed no difference between WT and *lak* in relative abundance of five distinct morphological cell types (Fig. 3.7).

To verify that our transplantations did not disrupt NT patterning of the retina and that solitary RGCs adopt appropriate positional fates, we analyzed *ephrin-A5b* expression as a specific marker for nasal RGCs (Fig. 3.3k, l; see Methods for details). In the WT^{*Brn3c:mGFP*}->WT retina, graded *ephrin-A5b* expression persists (Fig. 3.3m). In WT^{*Brn3c:mGFP*}->*lak* chimeras, small numbers of donor-derived RGCs visibly express *ephrin-A5b* in nasal locations, but not in the temporal retina ($n = 6$; Fig. 3.3n), consistent with models suggesting that retinal positional identity is specified prior to, and independent of, RGC genesis (Brennan *et al.* 1997; Kay *et al.* 2005; Picker *et al.* 1999).

Finally, we ruled out a delay of tectal innervation in WT^{*Brn3c:mGFP*}->*lak* chimeras by imaging chimeras at 80hpf, an early stage of RGC tectal innervation. RGC axons, tipped with growth cones were seen in the tecta of both WT and *lak* hosts (Fig. 3.3i, j). Combined, the axon arbor phenotype is unlikely to be a consequence of developmental differences of the tectum in WT^{*Brn3c:mGFP*}->*lak* chimeras, but rather is attributable to the difference in the density of RGC axons.

We predicted from the mapping functions of solitary axons (see Fig. 3.2d,e) that their arbors would be larger than those under crowded conditions. Indeed, morphometric analysis of arbor shapes revealed that solitary arbors cover a larger territory and have increased number and length branches (Fig. 3.4a, b). This increase in arbor size and complexity is already evident at 4 dpf and becomes more pronounced by 7 dpf, through the net addition of branches (Fig. 3.4c-e). These findings suggest that axonal arbors are

normally restricted in their initial size by the presence of other axons. This is consistent with the view that competition for target territory refines the map by suppressing or eliminating branches in retinotopically inappropriate territory (Ruthazer and Cline 2004). Importantly, solitary axons in zebrafish showed a positional bias – excessive branching occurred largely on the proximal side of the arbor (Fig. 3.4f).

In conclusion, our experimental results indicate that RGC axon-axon interactions, including competition, are largely dispensable for retinotopic targeting along the anterior-posterior axis. Although this does not rule out the possibility that competition can profoundly influence the map in a densely innervated tectum (Lemke and Reber 2005; Reber *et al.* 2004), our findings support a mapping mechanism that requires a second tectum-derived gradient, balancing the repellent signal provided by ephrin-As. This gradient, whether provided by growth-promoting effect of ephrin-A on nasal axons (Hansen *et al.* 2004), reverse chemorepellent signaling from tectally-expressed EphA to retinal axons (Rashid *et al.* 2005), or a different mechanism (Ichijo and Bonhoeffer 1998; von Boxberg *et al.* 1993), guides axons to the posterior tectum. Within the termination zone, axon-axon interactions then sculpt the axonal arbor and restrict branching along the length of the axon.

Methods

Generation of chimeras. WT donor embryos carrying the *Brn3c:mGFP* transgene (Xiao *et al.* 2005) were injected with a solution of 1-4% tetramethylrhodamine-conjugated dextran and 1-4% biotin-conjugated dextran (Invitrogen). Host embryos were collected from heterozygous *lak* carrier incrosses, or heterozygous male carriers mated to homozygous *lak* mutant females. Donor and host embryos were enzymatically dechorionated by incubation for 5-8 minutes in a solution of 0.5 mg/ml pronase (Sigma) in water. Chimeric embryos with rhodamine-positive clones in the neural retina were selected at 30-36 hpf, and raised in 0.2 mM phenylthiocarbamide (PTU) to inhibit melanin synthesis.

Smaller donor-derived clones, which are more likely to give rise to single RGCs, were found in locations biased toward the central retina, likely due to the proliferation of cells in the post-embryonic peripheral retina.

Immunohistochemistry. Larvae carrying <4 RGC axons were selected at 3, 4, or 7 dpf and stained for GFP and ZN5 as previously described (Xiao *et al.* 2005), with the following modifications: 80 hpf and 7 dpf larvae were permeabilized in 1 mg/ml collagenase in PBS for 1.5 and 2.5-3 hours, respectively. Anti-GFP and ZN5 antibodies were used at 1:2,000 and 1:400 dilutions, and donor-derived cells in 80 hpf and 7 dpf larvae were identified by reaction with alexa-fluor-conjugated avidin (Invitrogen).

Imaging and quantification. 4 dpf larvae were anesthetized and immobilized in 1% low melting point agarose. 7 dpf whole-mount stained larvae were mounted in ~90% glycerol.

Dorsal confocal stacks were collected with a BioRad MRC 1024 or Zeiss LSM Pascal microscope.

Custom-designed macros in Object-Image (available at <http://simon.bio.uva.nl/object-image.html>) were used for image analysis. Mapping functions were obtained blind to host genotype and retinal cell body position.

RGC soma position (%NT) was calculated as the percentage of distance from the nasal pole of the retina along the nasotemporal axis (Fig. 3.6a-c):

$$\%NT = [(NT_{max} - NT_{DV})/2 + NT_{cell}]/NT_{max} * 100,$$

where NT_{max} is the maximum distance from nasal to temporal locations in the ganglion cell layer, NT_{DV} is the distance from nasal to temporal poles at the dorsal-ventral position of the cell, and NT_{cell} is the distance from the nasal pole to the cell body. (All distances were measured as curved lines along the inner plexiform layer, as visualized with ZN5 reactivity.)

Tectal positions were measured as the percentage of the distance between the anterior and posterior poles of the tectum, demarcated by extent of ZN5 label (Fig. 3.6d-f).

Summary retinotectal mapping functions were assembled for 7 dpf larvae with 30 RGCs in 27 $WT^{Brn3c:mGFP} \rightarrow WT$ chimera eyes, and 19 RGCs in 18 $WT^{Brn3c:mGFP} \rightarrow lak$ chimera eyes.

Individual axon arbors were imaged at 4 dpf or 7 dpf and analyzed using Object-Image, blind to host genotype, as previously described (Smear *et al.* 2007). Axon arbor stick-

figures were exported directly from morphometric analysis and prepared using Adobe Photoshop.

In situ hybridization. Dig-labeled EphA4b antisense probes were synthesized *in vitro* as published (Picker *et al.* 1999). Whole-mount in situ hybridization was performed as previously described (Kay *et al.* 2005). For sections, larvae were mounted in gelatin/albumin and cut with a Leica vibratome to 25 μm . Stained embryos were imaged using a SPOT CCD camera mounted on a Leica dissecting microscope or Zeiss compound microscope with DIC optics, and prepared using Adobe Photoshop.

Single cell electroporation and morphological analysis. Small numbers of neurons were labeled in live larvae using a method adapted from Haas *et al.* (2001). Tectal cells were transfected with either α -*tubulin:GFP*, *eF1 α :GFP*, or mixed α -*tubulin:gal4;UAS:GFP* plasmids at a DNA concentration of 1.5 $\mu\text{g}/\mu\text{l}$. WT and *lak* mutant larvae were electroporated at 4 or 5 dpf and imaged as above at 6 or 7 dpf. ‘Palm cells’: Cell bodies are located near the tectal midline, neurites in the tectal neuropil. ‘Vine cells’: Cell bodies are located in the tectum, arbors extend to more ventral brain structures. Glial-like ‘giant kelp cells’: Cell bodies are directly apposed to the tectal midline; endfeet are at the dorsal surface of the brain, superficial to RGC input layers.

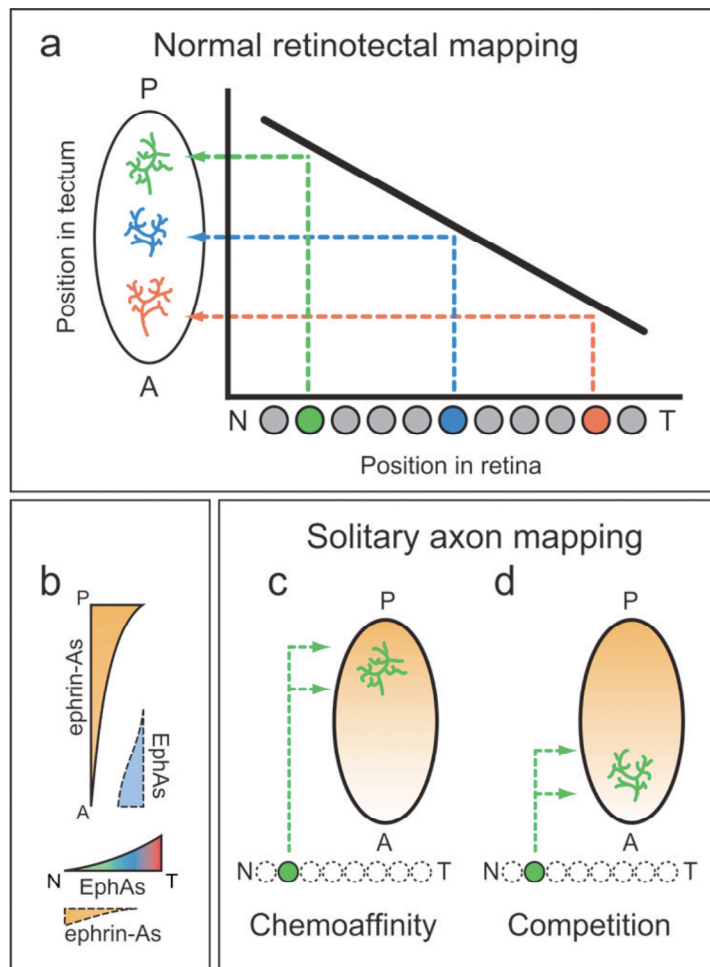


Figure 3.1: Two potential mechanisms for formation of the retinotectal map.

a, Graphical representation of the retinotectal mapping function. Retinal ganglion cells (RGCs) at increasingly nasal positions project axons to increasingly posterior regions of the optic tectum.

b, Gradients of tectal ephrin-A ligands and retinal EphA receptors repel axons from the posterior tectum.

In addition, retina and tectum express countergradients of ephrin-A and EphA, respectively. **c, d.** Hypothetical maps formed by solitary axons. If chemoaffinity (**c**) between axons and targets guides retinotectal mapping then solitary nasal axons retain projections to posterior tectum. If axon-axon competition (**d**) drives nasal axons to posterior tectum then solitary axons should terminate in the anterior tectum, where ephrin-A signalling is lowest.

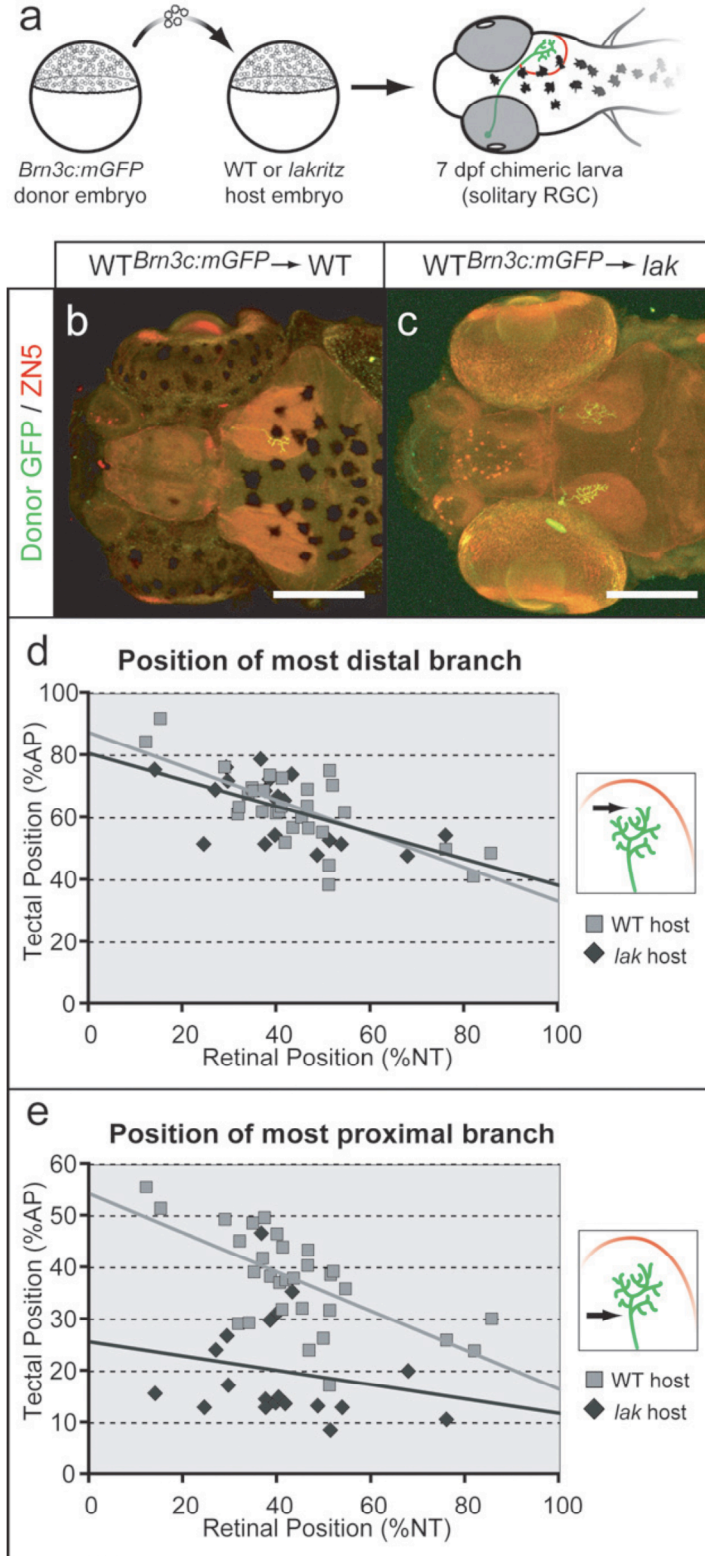


Figure 3.2: Retinotectal mapping functions in the presence or absence of axon-axon interactions.

a, Cell transplantation from WT donors into RGC-deficient *lak* mutants gives rise to chimeras with single, labelled RGC axons (green) that project to the optic tectum (red outline).

b, c, 7 dpf chimeric larvae, immunostained to highlight RGC axon arbors (green) and to reveal tectal neuropil (red, stained with Zn5). **b**, $WT^{Brn3c:mGFP-}$ >WT chimera containing a single RGC axon arbor terminating on the right tectum. Scale bar: 200 μ m.

c, $WT^{Brn3c:mGFP-}>lak$ chimera, with a single arbor

on left tectum, two fainter arbors on the right tectum. Note that the arbors terminate beyond the anterior margin of the tectum. Scale bar: 200 μm . **d, e**, Retinotectal mapping functions for 7 dpf chimeras. Distal-most extension of RGC axon arbors (**d**) shows no difference between axons in $\text{WT}^{\text{Brn3c:mGFP}} \rightarrow \text{WT}$ and $\text{WT}^{\text{Brn3c:mGFP}} \rightarrow \text{lak}$ chimeras. Proximal-most branches (**e**) show a significant anterior shift in $\text{WT}^{\text{Brn3c:mGFP}} \rightarrow \text{lak}$ chimeras. Scale: 100% AP is 180 μm .

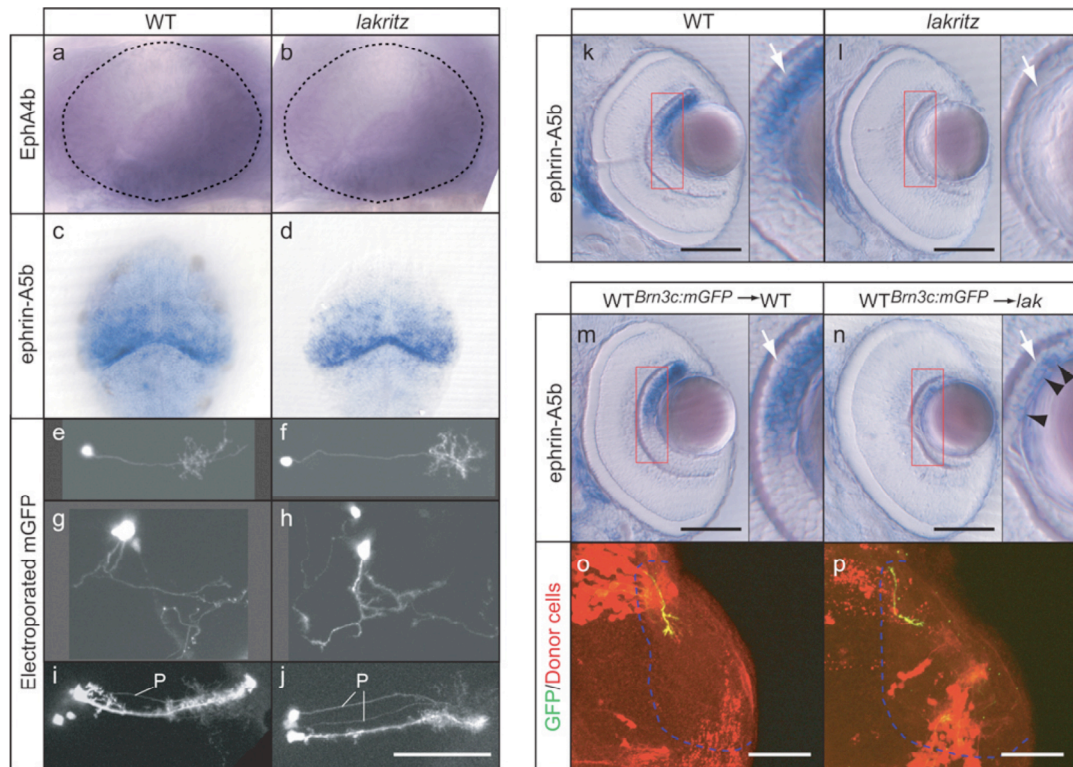
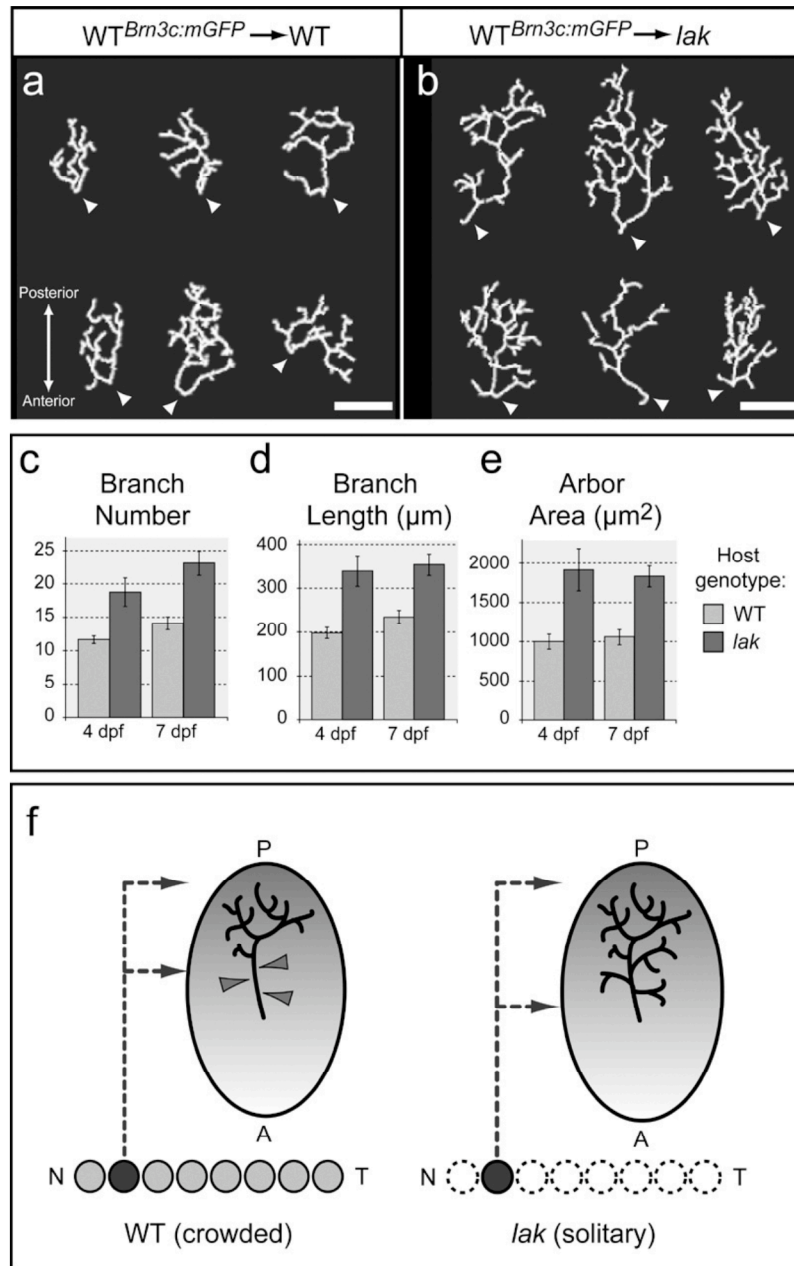


Figure 3.3: Evidence for normal patterning of retina and tectum in *lak* mutants.

a, b, Temporal retinal EphA4b expression in 28 hpf WT (a) and *lak* (b) eyes. Optic fissure is at lower left. **e-j,** Cellular composition of the tectum, visualized by transfected GFP, is similar in WT (e, g, i) and *lak* mutant larvae (f, h, j). Descriptions of cell morphologies in Methods. Scale bar: 100 μ m. ‘Palm cells’ (c, d). ‘Vine cells’ (e, f). ‘Giant kelp cells’ (g, h). Neighboring palm cells marked with ‘P’. **k-n,** ephrin-A5b expression in 80hpf larvae. Red box is inset at right, scale bar: 100 μ m. Expression is seen in nasal RGCs in WT (k), but completely absent in *lak* mutants (l). Expression is unaffected in WT host chimeras (m). Small numbers of donor-derived nasal RGCs express ephrin-A5b in *lak* mutant hosts (n), suggesting that appropriate positional identity is adopted in the mutant environment independent of RGC density. **o, p,** Labeling of

single axons at 80 hpf in WT (o) and *lak* (p). A solitary growth cone (p) extends into the tectum (blue outline) at this early stage, demonstrating that innervation is not generally delayed. Scale bar: 50 μm .



anterior down. Scale bar: 50 μm . **c-e**, Quantification of 4 dpf and 7 dpf arbors in WT and *lak* host chimeras. At both 4 dpf and 7 dpf, solitary arbors have significantly increased numbers of branches (**c**), total branch length (**d**), and area (**e**). Graphs are mean \pm SEM. For all 4 dpf, $p < 0.01$ (two-tailed t-test, $n = 17$ WT hosts, $n = 8$ *lak* hosts). For all 7 dpf,

Figure 3.4: Axon-axon competition restricts axon arbor size and complexity.

a, b, Examples of 7 dpf GFP-labeled axon arbors.

Arbors found in WT $Brn3c:mGFP \rightarrow WT$ chimeras (**a**) are smaller, with fewer

and shorter branches, than arbors found in

WT $Brn3c:mGFP \rightarrow lak$ chimeras (**b**).

Orientation: posterior up,

$p < 0.01$ (two-tailed t-test, $n=19$ WT, $n=19$ *lak*). **f**, Proposed role for axon-axon interactions during retinotectal map formation. Distal (posterior) projections of axon arbors are unaffected by a loss of neighboring axons. Proximal branches are pruned (triangle tips) by competition with other axons, but persist in solitary arbors (right).

Movie 3.5 available at <http://XXXXXXXXXXXXXXXXXXXX>

Movie 3.5: RGC axon pathfinding errors during retinal exit in WT^{Brn3c:mGFP}->*lak* chimeras.

Dorsal confocal stack of 7 dpf WT^{Brn3c:mGFP}->*lak* chimera with ~5 RGCs in varying retinal positions projecting axons. One axon (blue arrow), is visible exiting the retina, but peripheral RGC axons meander and branch in aberrant directions (red arrows).

Similar errors were seen in <5% of WT^{Brn3c:mGFP}->*lak* chimeras with one or more axons projecting to the tectum. Orientation: nasal up, temporal down.

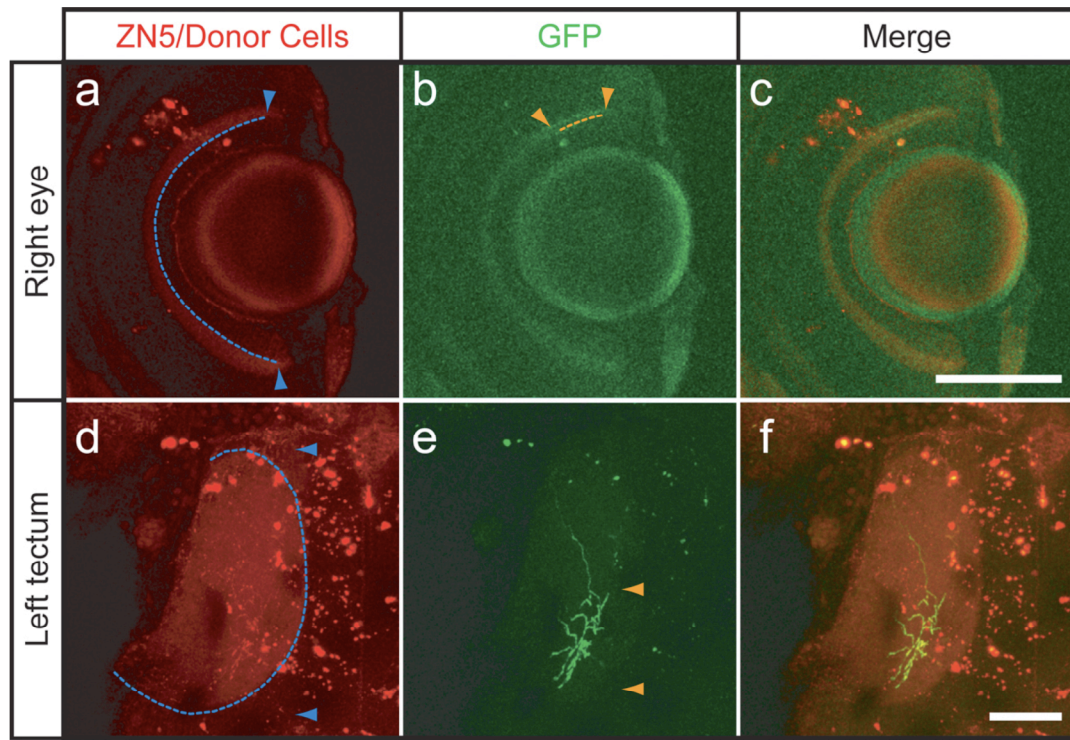


Figure 3.6: Example quantification of retinal and tectal position in a single chimeric larva.

a-c, Retinal quantification. Single optical section from dorsal confocal imaging of 7 dpf $WT^{Brn3c:mGFP} \rightarrow WT$ chimera. Orientation: nasal - up, medial - left. **a,** ZN5-immunoreactive RGC fibers are seen in the ganglion cell layer (GCL), and donor-derived cells (including one RGC) are distributed in characteristic radial clones. In this chimera, the optical section containing the RGC corresponds with the optical section with the greatest distance from nasal to temporal poles ($NT_{max} = NT_{DV}$, blue dashed line, see Methods). **b,** Same optical section, imaged for GFP immunoreactivity. The GFP-positive, single RGC soma is visible in the GCL. The cells lies 15% of the distance from nasal to temporal poles (NT_{cell} , orange dashed line). **c,** Merged images from a, b. Scale

bar: 100 μm . **d-f**, Tectal quantification. Dorsal confocal projection of 7 dpf contralateral tectum as described in a-c. Orientation: anterior - up, lateral - left. **d**, Extent of the tectal neuropil (outlined in dashed blue, 0% and 100% denoted with arrowheads) is visualized by ZN5 staining. Donor-derived tectal palm cell bodies appear as saturated red. **e**, GFP positive single RGC arbor. Distal-most branch tip (bottom orange arrowhead) and proximal-most branch (top orange arrowhead) are at 92 and 51 %AP, respectively. **f**, Merged images from d, e. Scale bar: 50 μm .

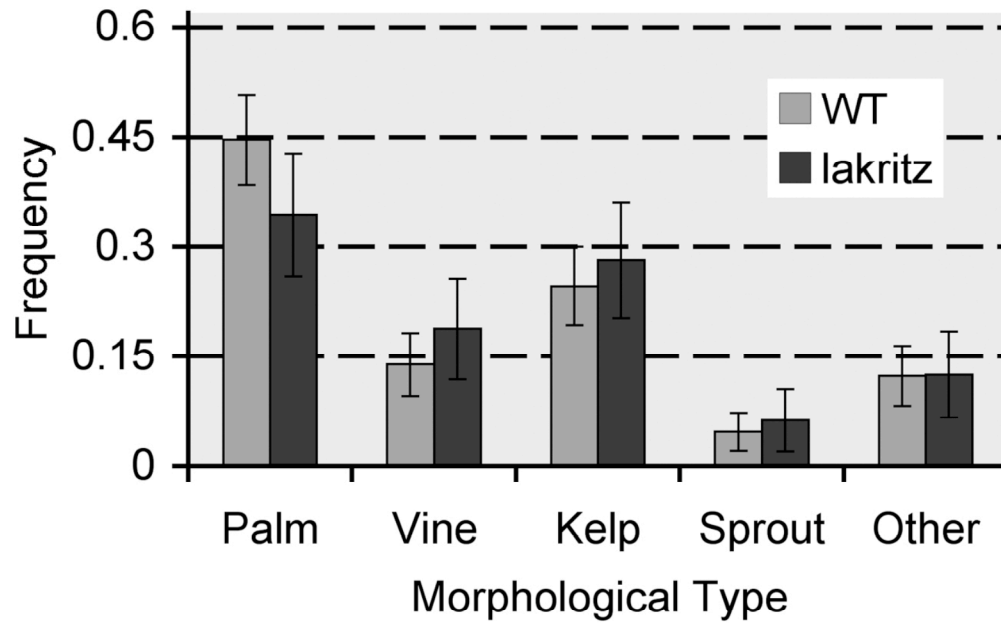


Figure 3.7: Frequency of cell types identified by single cell electroporation in WT and *lakritz* larvae.

Histogram showing frequency (+/- standard error) of cells found in 5 morphologically distinct categories. All classes of cells were present at similar frequencies among WT (n=65) and *lakritz* (n=32) populations. To avoid sampling bias, clusters of same-type cells were counted as single instances.

Acknowledgments We thank Tong Xiao (UCSF), Alexander Picker (MPICBG Dresden), Uwe Drescher (King's College, London), Kurt Haas (UBC) and Holly Cline (Cold Spring Harbor Laboratory) for reagents and advice, Julie Pinkston-Gosse and members of the Baier Lab for review of the manuscript. This work was supported by the NIH (HB, NG) and a March of Dimes Research Grant (HB).

CHAPTER 4

RGC AXON LAMINATION DOES NOT REQUIRE RGC-RGC INTERACTIONS

In addition to the topographic organization along the AP and DV axes, retinal input to the tectum is organized into distinct layers. In the larval zebrafish, as in adult goldfish, there are four retinorecipient laminae (VON BARTHELD and MEYER 1987; XIAO *et al.* 2005). While recent progress has been made, e.g. (XIAO and BAIER 2007), compared to topographic mapping, far less is known what factors drive laminar organization during development of the retinotectal projection.

To test whether axon-axon interactions are necessary for establishment or maintenance of tectal lamination, I asked whether solitary axons have normal laminar structure. Comparing the axon arbor morphology in WT->WT and WT->*lakritz* chimeras from chapter 3, I found that laminar organization persists in the absence of axon-axon interactions.

RGCs expressing the *Brn3c:mGFP* transgene project to the stratum opticum (SO) and all three sublaminae of the stratum fibrosum et griseum superficiale (SFGS) (XIAO *et al.* 2005). These axons elaborate arbors in one specific sublamina, and do not branch between layers (XIAO and BAIER 2007). Similarly, in WT^{*Brn3c:mGFP*}->WT chimeras, GFP-positive axons are found in the SO, or more commonly, in the SFGS (Table 4.1), and restrict branches to a single layer (Figure 4.1a,c). Interestingly, solitary axons in

WT^{Bm3e:mGFP}->*lak* chimeras are indistinguishable from those in WT hosts. Arbors are restricted to one layer (Figure 4.1b,d), and show similar frequencies of SO and SFGS innervation (Table 4.1). These findings suggest that axon-axon interactions are dispensable for development of laminar specificity during tectal innervation of RGC afferents.

Methods:

Image analysis. Dorsal confocal stacks obtained for single arbor morphological or mapping analysis (4dpf and 7dpf - chapter 3) were analyzed. Laminar identity of each axon was assigned by assessing arbor position relative to autofluorescent skin (very near = SO, farther = SFGS).

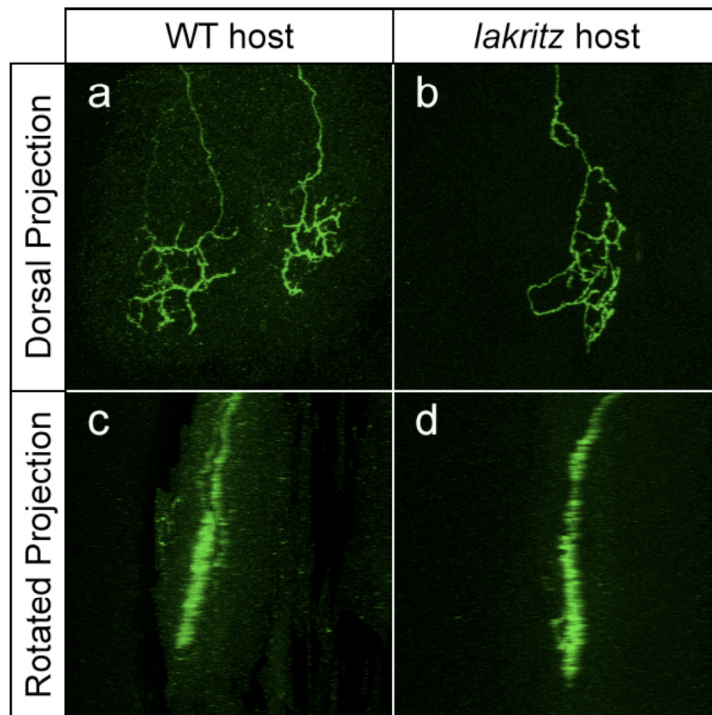


Figure 4.1: Single axon laminar choice in WT and *lak* hosts. **a,b**, Dorsal confocal projections of GFP-labeled axons in WT (a) and *lakritz* (b) hosts. Anterior up, lateral left. **c,d**, Rotated projections show that each axon occupies a single layer within the tectal neuropil.

4 dpf chimeras	Arbors in SO	Arbors in SFGS	Table 4.1: Number of RGC axon arbors terminating in SO and SFGS at 4 and 7dpf. Frequency of SO and SFGS innervation is not significantly different between RGC axons
WT hosts	9 (23%)	30 (77%)	
<i>lakritz</i> hosts	5 (31%)	11 (69%)	
7 dpf chimeras	Arbors in SO	Arbors in SFGS	
WT hosts	13 (20%)	52 (80%)	
<i>lakritz</i> hosts	8 (24%)	26 (76%)	

in WT and *lakritz* hosts at either 4dpf ($p=0.225$) or 7dpf ($p=0.344$).

CHAPTER 5

FUTURE DIRECTIONS AND CONCLUDING REMARKS

In this thesis, I aimed to understand the development of the retinotectal projection as a means to further our understanding of how the nervous system maintains faithful representation of sensory signals. Specifically, I have focused on two key events in the development of the retinotectal map: establishment of positional identity, and innervation of the tectum in a topographically organized manner.

By focusing on the patterning of the retina along the DV axis, we uncovered a role for *radar* as a required factor for dorsal retina specification and subsequent ventral tectum innervation. Further studies with the *radar* gene will help to refine the mechanisms of dorsal specification, and resolve outstanding questions. Of particular interest is how the residual DV patterning of the retinotectal map is established. Are other BMP-family genes compensating for the loss of *radar* in *s327* mutants? Are there ‘ventralizing’ factors that play analogous but opposite roles in patterning the ventral retina? In chick, ventroptin has been identified as a BMP antagonist that leads to ventral specification. Is a similar mechanism at work in zebrafish? Does it merely antagonize dorsal BMP signaling, or can it specify ventral fate through a BMP-independent mechanism?

Other questions address potential different roles for *radar* at different stages of development. Why does the absence of *radar* lead to increased retinal cell death? Is this

part of a pathway that helps to regulate the size of the retina? When, specifically, does *radar* bestow dorsal retinal fate? Does it serve only to initiate dorsal *bmp2b* and *bmp4* expression? Or is prolonged *radar* expression required to maintain *tbx2b* and *tbx5* expression? Can ventral RGCs be reprogrammed by *radar* expression after differentiation to express dorsal cell markers (e.g. *ephrin-b2a*)? Are late-differentiating RGCs, derived from the ciliary marginal zone, also dependent on *radar* for dorsalization? These and other questions, likely addressable with the genetic and transgenic tools in zebrafish, will help to nail down the function and importance of *radar*.

The second major focus of my thesis was to determine the importance of RGC-RGC interactions in driving retinotopic map formation in the zebrafish tectum. As axon-axon interactions had been proposed as one means of driving posterior growth (up the repellent ephrin-A gradient), it was surprising to find that the distal retinotectal mapping function is unchanged in solitary RGCs (in WT->*lak* chimeras - figure 3.2). The fact that ectopic anterior branches are present in solitary RGC axon arbors (figure 3.4) suggests that there are important roles for RGC-RGC interactions in refinement of individual arbors.

These findings are indeed quite revealing, as in ‘revealing many more questions’. What is the nature of the second, tectum-derived gradient that drives axons toward the posterior pole? This is a particularly difficult question to answer, as disrupting the mechanisms that have been proposed to drive posterior growth (e.g. adhesive or attractive EphA/ephrin-A interactions) may also affect other dimensions of map development. More accessible may be the RGC-RGC-dependent mechanisms that eliminate proximal

branches. To what extent are branches maintained based on competition for trophic factors? Is proximal pruning dependent on activity-dependent competitive mechanisms?

Finally, further exploration of the molecules responsible for laminar choice may be possible using similar GFP-labeled transplanted cells. While screening large numbers of candidate genes could be laborious, MO-mediated knockdown or mutant Brn3c:mGFP cells transplanted into WT hosts could identify new players in laminar targeting.

Following up on these questions will add to the growing and important body of work on the development of the vertebrate retinotectal projection, an important model for sensory system topographic mapping. It is my hope that the studies presented here will compel follow-up work to address these and other questions, ultimately advancing the field toward a functional understanding -- one that will make the leap from academic understanding to clinical application.

REFERENCES

- Asai-Coakwell, M., C. R. French, K. M. Berry, M. Ye, R. Koss *et al.*, 2007 GDF6, a novel locus for a spectrum of ocular developmental anomalies. *Am J Hum Genet* **80**: 306-315.
- Baier, H., S. Klostermann, T. Trowe, R. O. Karlstrom, C. Nusslein-Volhard *et al.*, 1996 Genetic dissection of the retinotectal projection. *Development* **123**: 415-425.
- Barbieri, A. M., G. Lupo, A. Bulfone, M. Andreazzoli, M. Mariani *et al.*, 1999 A homeobox gene, *vax2*, controls the patterning of the eye dorsoventral axis. *Proc Natl Acad Sci U S A* **96**: 10729-10734.
- Behesti, H., J. K. Holt and J. C. Sowden, 2006 The level of BMP4 signaling is critical for the regulation of distinct T-box gene expression domains and growth along the dorso-ventral axis of the optic cup. *BMC Dev Biol* **6**: 62.
- Bonhoeffer, F., and J. Huf, 1980 Recognition of cell types by axonal growth cones in vitro. *Nature* **288**: 162-164.
- Brennan, C., B. Monschau, R. Lindberg, B. Guthrie, U. Drescher *et al.*, 1997 Two Eph receptor tyrosine kinase ligands control axon growth and may be involved in the creation of the retinotectal map in the zebrafish. *Development* **124**: 655-664.
- Carvalho, R. F., M. Beutler, K. J. Marler, B. Knoll, E. Becker-Barroso *et al.*, 2006 Silencing of EphA3 through a cis interaction with ephrinA5. *Nat Neurosci* **9**: 322-330.
- Chang, C., and A. Hemmati-Brivanlou, 1999 *Xenopus* GDF6, a new antagonist of noggin and a partner of BMPs. *Development* **126**: 3347-3357.

- Davis, R. E., and B. E. Schlumpf, 1984 Visual recovery in goldfish following unilateral optic tectum ablation: evidence of competition between optic axons for tectal targets. *Behav Brain Res* **13**: 287-291.
- Dyer, M. A., and C. L. Cepko, 2001 Regulating proliferation during retinal development. *Nat Rev Neurosci* **2**: 333-342.
- Flanagan, J. G., 2006 Neural map specification by gradients. *Curr Opin Neurobiol* **16**: 59-66.
- Fraser, S. E., and D. H. Perkel, 1990 Competitive and positional cues in the patterning of nerve connections. *J Neurobiol* **21**: 51-72.
- Gierer, A., 1983 Model for the retino-tectal projection. *Proc R Soc Lond B Biol Sci* **218**: 77-93.
- Goodhill, G. J., 2007 Contributions of theoretical modeling to the understanding of neural map development. *Neuron* **56**: 301-311.
- Goodhill, G. J., and J. Xu, 2005 The development of retinotectal maps: a review of models based on molecular gradients. *Network* **16**: 5-34.
- Goutel, C., Y. Kishimoto, S. Schulte-Merker and F. Rosa, 2000 The ventralizing activity of Radar, a maternally expressed bone morphogenetic protein, reveals complex bone morphogenetic protein interactions controlling dorso-ventral patterning in zebrafish. *Mech Dev* **99**: 15-27.
- Hansen, M. J., G. E. Dallal and J. G. Flanagan, 2004 Retinal axon response to ephrin-as shows a graded, concentration-dependent transition from growth promotion to inhibition. *Neuron* **42**: 717-730.

- Harada, T., C. Harada and L. F. Parada, 2007 Molecular regulation of visual system development: more than meets the eye. *Genes Dev* **21**: 367-378.
- Hayes, W. P., and R. L. Meyer, 1988 Optic synapse number but not density is constrained during regeneration onto surgically halved tectum in goldfish: HRP-EM evidence that optic fibers compete for fixed numbers of postsynaptic sites on the tectum. *J Comp Neurol* **274**: 539-559.
- Hindges, R., T. McLaughlin, N. Genoud, M. Henkemeyer and D. D. O'Leary, 2002 EphB forward signaling controls directional branch extension and arborization required for dorsal-ventral retinotopic mapping. *Neuron* **35**: 475-487.
- Honda, H., 2003 Competition between retinal ganglion axons for targets under the servomechanism model explains abnormal retinocollicular projection of Eph receptor-overexpressing or ephrin-lacking mice. *J Neurosci* **23**: 10368-10377.
- Hornberger, M. R., D. Dutting, T. Ciossek, T. Yamada, C. Handwerker *et al.*, 1999 Modulation of EphA receptor function by coexpressed ephrinA ligands on retinal ganglion cell axons. *Neuron* **22**: 731-742.
- Hua, J. Y., M. C. Smear, H. Baier and S. J. Smith, 2005 Regulation of axon growth in vivo by activity-based competition. *Nature* **434**: 1022-1026.
- Ichijo, H., and F. Bonhoeffer, 1998 Differential withdrawal of retinal axons induced by a secreted factor. *J Neurosci* **18**: 5008-5018.
- Imai, Y., and W. S. Talbot, 2001 Morpholino phenocopies of the *bmp2b/swirl* and *bmp7/snailhouse* mutations. *Genesis* **30**: 160-163.
- Kay, J. N., K. C. Finger-Baier, T. Roeser, W. Staub and H. Baier, 2001 Retinal ganglion cell genesis requires *lakritz*, a Zebrafish atonal Homolog. *Neuron* **30**: 725-736.

- Kay, J. N., B. A. Link and H. Baier, 2005 Staggered cell-intrinsic timing of *ath5* expression underlies the wave of ganglion cell neurogenesis in the zebrafish retina. *Development* **132**: 2573-2585.
- Knapik, E. W., A. Goodman, M. Ekker, M. Chevrette, J. Delgado *et al.*, 1998 A microsatellite genetic linkage map for zebrafish (*Danio rerio*). *Nat Genet* **18**: 338-343.
- Koshiba-Takeuchi, K., J. K. Takeuchi, K. Matsumoto, T. Momose, K. Uno *et al.*, 2000 Tbx5 and the retinotectum projection. *Science* **287**: 134-137.
- Lemke, G., and M. Reber, 2005 Retinotectal mapping: new insights from molecular genetics. *Annu Rev Cell Dev Biol* **21**: 551-580.
- Mann, F., S. Ray, W. Harris and C. Holt, 2002 Topographic mapping in dorsoventral axis of the *Xenopus* retinotectal system depends on signaling through ephrin-B ligands. *Neuron* **35**: 461-473.
- McLaughlin, T., R. Hindges and D. D. O'Leary, 2003 Regulation of axial patterning of the retina and its topographic mapping in the brain. *Curr Opin Neurobiol* **13**: 57-69.
- Mintzer, K. A., M. A. Lee, G. Runke, J. Trout, M. Whitman *et al.*, 2001 Lost-a-fin encodes a type I BMP receptor, Alk8, acting maternally and zygotically in dorsoventral pattern formation. *Development* **128**: 859-869.
- Monschau, B., C. Kremoser, K. Ohta, H. Tanaka, T. Kaneko *et al.*, 1997 Shared and distinct functions of RAGS and ELF-1 in guiding retinal axons. *Embo J* **16**: 1258-1267.

- Mui, S. H., R. Hindges, D. D. O'Leary, G. Lemke and S. Bertuzzi, 2002 The homeodomain protein Vax2 patterns the dorsoventral and nasotemporal axes of the eye. *Development* **129**: 797-804.
- Muto, A., M. B. Orger, A. M. Wehman, M. C. Smear, J. N. Kay *et al.*, 2005 Forward genetic analysis of visual behavior in zebrafish. *PLoS Genet* **1**: e66.
- Neuhauss, S. C., O. Biehlmaier, M. W. Seeliger, T. Das, K. Kohler *et al.*, 1999 Genetic disorders of vision revealed by a behavioral screen of 400 essential loci in zebrafish. *J Neurosci* **19**: 8603-8615.
- Picker, A., C. Brennan, F. Reifers, J. D. Clarke, N. Holder *et al.*, 1999 Requirement for the zebrafish mid-hindbrain boundary in midbrain polarisation, mapping and confinement of the retinotectal projection. *Development* **126**: 2967-2978.
- Poggi, L., M. Vitorino, I. Masai and W. A. Harris, 2005 Influences on neural lineage and mode of division in the zebrafish retina in vivo. *J Cell Biol* **171**: 991-999.
- Pyati, U. J., A. E. Webb and D. Kimelman, 2005 Transgenic zebrafish reveal stage-specific roles for Bmp signaling in ventral and posterior mesoderm development. *Development* **132**: 2333-2343.
- Rashid, T., A. L. Upton, A. Blentic, T. Ciossek, B. Knoll *et al.*, 2005 Opposing gradients of ephrin-As and EphA7 in the superior colliculus are essential for topographic mapping in the mammalian visual system. *Neuron* **47**: 57-69.
- Reber, M., P. Burrola and G. Lemke, 2004 A relative signalling model for the formation of a topographic neural map. *Nature* **431**: 847-853.

- Rissi, M., J. Wittbrodt, E. Delot, M. Naegeli and F. M. Rosa, 1995 Zebrafish Radar: a new member of the TGF-beta superfamily defines dorsal regions of the neural plate and the embryonic retina. *Mech Dev* **49**: 223-234.
- Roeser, T., and H. Baier, 2003 Visuomotor behaviors in larval zebrafish after GFP-guided laser ablation of the optic tectum. *J Neurosci* **23**: 3726-3734.
- Ruthazer, E. S., and H. T. Cline, 2004 Insights into activity-dependent map formation from the retinotectal system: a middle-of-the-brain perspective. *J Neurobiol* **59**: 134-146.
- Sakuta, H., H. Takahashi, T. Shintani, K. Etani, A. Aoshima *et al.*, 2006 Role of bone morphogenic protein 2 in retinal patterning and retinotectal projection. *J Neurosci* **26**: 10868-10878.
- Schauerte, H. E., F. J. van Eeden, C. Fricke, J. Odenthal, U. Strahle *et al.*, 1998 Sonic hedgehog is not required for the induction of medial floor plate cells in the zebrafish. *Development* **125**: 2983-2993.
- Schmidt, J., and T. Cohn, 1995 Changes in retinal arbors in compressed projections to half tecta in goldfish. *J Neurobiol* **28**: 409-418.
- Schulte, D., T. Furukawa, M. A. Peters, C. A. Kozak and C. L. Cepko, 1999 Misexpression of the Emx-related homeobox genes *cVax* and *mVax2* ventralizes the retina and perturbs the retinotectal map. *Neuron* **24**: 541-553.
- Scott, E. K., L. Mason, A. B. Arrenberg, L. Ziv, N. J. Gosse *et al.*, 2007 Targeting neural circuitry in zebrafish using GAL4 enhancer trapping. *Nat Methods* **4**: 323-326.
- Shimoda, N., E. W. Knapik, J. Ziniti, C. Sim, E. Yamada *et al.*, 1999 Zebrafish genetic map with 2000 microsatellite markers. *Genomics* **58**: 219-232.

- Shin, D., C. H. Shin, J. Tucker, E. A. Ober, F. Rentzsch *et al.*, 2007 Bmp and Fgf signaling are essential for liver specification in zebrafish. *Development* **134**: 2041-2050.
- Sidi, S., C. Goutel, N. Peyrieras and F. M. Rosa, 2003 Maternal induction of ventral fate by zebrafish radar. *Proc Natl Acad Sci U S A* **100**: 3315-3320.
- Smear, M. C., H. W. Tao, W. Staub, M. B. Orger, N. J. Gosse *et al.*, 2007 Vesicular glutamate transport at a central synapse limits the acuity of visual perception in zebrafish. *Neuron* **53**: 65-77.
- Sperry, R. W., 1963 Chemoaffinity in the Orderly Growth of Nerve Fiber Patterns and Connections. *Proc Natl Acad Sci U S A* **50**: 703-710.
- Stuermer, C. A., 1988 Retinotopic organization of the developing retinotectal projection in the zebrafish embryo. *Journal of Neuroscience* **8**: 4513-4530.
- Take-uchi, M., J. D. Clarke and S. W. Wilson, 2003 Hedgehog signalling maintains the optic stalk-retinal interface through the regulation of Vax gene activity. *Development* **130**: 955-968.
- Tsigankov, D. N., and A. A. Koulakov, 2006 A unifying model for activity-dependent and activity-independent mechanisms predicts complete structure of topographic maps in ephrin-A deficient mice. *J Comput Neurosci* **21**: 101-114.
- von Bartheld, C. S., and D. L. Meyer, 1987 Comparative neurology of the optic tectum in ray-finned fishes: patterns of lamination formed by retinotectal projections. *Brain Res* **420**: 277-288.


- von Boxberg, Y., S. Deiss and U. Schwarz, 1993 Guidance and topographic stabilization of nasal chick retinal axons on target-derived components in vitro. *Neuron* **10**: 345-357.
- Wehman, A. M., W. Staub, J. R. Meyers, P. A. Raymond and H. Baier, 2005 Genetic dissection of the zebrafish retinal stem-cell compartment. *Dev Biol* **281**: 53-65.
- Willshaw, D., 2006 Analysis of mouse EphA knockins and knockouts suggests that retinal axons programme target cells to form ordered retinotopic maps. *Development* **133**: 2705-2717.
- Xiao, T., and H. Baier, 2007 Lamina-specific axonal projections in the zebrafish tectum require the type IV collagen Dragnet. *Nat Neurosci* **10**: 1529-1537.
- Xiao, T., T. Roeser, W. Staub and H. Baier, 2005 A GFP-based genetic screen reveals mutations that disrupt the architecture of the zebrafish retinotectal projection. *Development* **132**: 2955-2967.
- Yates, P. A., A. D. Holub, T. McLaughlin, T. J. Sejnowski and D. D. O'Leary, 2004 Computational modeling of retinotopic map development to define contributions of EphA-ephrinA gradients, axon-axon interactions, and patterned activity. *J Neurobiol* **59**: 95-113.
- Zhang, X. M., and X. J. Yang, 2001 Temporal and spatial effects of Sonic hedgehog signaling in chick eye morphogenesis. *Dev Biol* **233**: 271-290.

PUBLISHING AGREEMENT

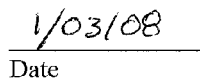
It is the policy of the University to encourage the distribution of all theses and dissertations. Copies of all UCSF theses and dissertations will be routed to the library via the Graduate Division. The library will make all theses and dissertations accessible to the public and will preserve these to the best of their abilities, in perpetuity.

Please sign the following statement:

I hereby grant permission to the Graduate Division of the University of California, San Francisco to release copies of my thesis or dissertation to the Campus Library to provide access and preservation, in whole or in part, in perpetuity.



Author Signature



Date